# Manuscript Details

| | |
|---|---|
| **Manuscript number** | JQSR_2019_262 |
| **Title** | The chronological, sedimentary and environmental context for the archaeological deposits at Blombos Cave, South Africa |
| **Article type** | Research Paper |


**Abstract**

The site of Blombos Cave (BBC) is well known for archaeological remains that have advanced our understanding of the development of modern human behaviour during the Middle Stone Age (MSA). Occupation of the cave occurred against a backdrop of landscape-scale environmental and sedimentary processes that provide the broader context for finer-scale interpretations of the site-formation history and archaeological patterns detected in the cave deposits. Aeolian and palaeosol sequences are abundant in the vicinity of BBC and these provide a partial view of the past landscapes available to the inhabitants of the cave. An important extension to the palaeo-landscape around BBC currently lies submerged on the Agulhas Bank, as sea levels were lower than at present for the entire period of human occupation of BBC. In this paper, we revisit the optically stimulated luminescence (OSL) chronology for the full sequence of sediment deposition inside BBC, increasing the number of dated samples to a total of 40 and revising the period of MSA occupation to between 97.7 ± 7.6 and 71.0 ± 5.7 ka (uncertainties at 95.4% probability). We describe the geological successions at four main areas around BBC, estimate the time of sediment deposition using OSL, and describe and interpret three seismic profiles on the Agulhas Bank, offshore of BBC. By correlating these onshore and offshore geological sequences with the sedimentary deposits inside BBC, we place the archaeological record within a landscape-scale chrono-stratigraphic framework to examine how environmental changes may have regulated the presence or absence of humans in the cave and surrounding terrain between about 100 and 70 ka.



| | |
|---|---|
| **Keywords** | Pleistocene; Sea Level Changes; South Atlantic; Geomorphology, coastal; Optical methods; optical dating; Bayesian age model; relative sea level; palaeo-Agulhas Plain; human–environment interactions |



| | |
|---|---|
| **Corresponding Author** | Zenobia Jacobs |
| **Corresponding Author's Institution** | University of Wollongong |
| **Order of Authors** | Zenobia Jacobs, Brian Jones, Hayley Cawthra, Christopher Henshilwood, Richard Roberts |
| **Suggested reviewers** | charles bristow, Craig Sloss, mark bateman, Brendan Brooke, Greg Botha |


## Submission Files Included in this PDF

**File Name [File Type]**

Cover letter.docx [Cover Letter]

Jacobs et al_text, references and captions_final.docx [Manuscript File]

Jacobs et al_figures_final.docx [Figure]

Jacobs et al_tables.docx [Table]

To view all the submission files, including those not included in the PDF, click on the manuscript title on your EVISE Homepage, then click 'Download zip file'.

## Research Data Related to this Submission

There are no linked research data sets for this submission. The following reason is given:
Data will be made available on request

School of Earth, Atmospheric and Life Sciences
University of Wollongong
Northfields Avenue
Wollongong
NSW 2522
Australia

11 April 2019

Dear Editor

We would like to submit the paper "*The chronological, sedimentary and environmental context for the archaeological deposits at Blombos Cave, South Africa*" for your consideration.

Blombos Cave contains the largest and best preserved Still Bay assemblages of any site in southern Africa, and finds from this site, including engraved ochres, shell beads, ochre containers and bone points, have revolutionised our thinking about the origins of modern human behaviour in the last decade. Much effort has been afforded to obtaining a reliable chronology for the Blombos Cave deposits. One shortcoming of the Blombos chronology, however, is that very few ages exist for the lower levels and none of the work has so far been placed within the wider landscape context in which the site is located. In this paper, we overcome this problem by revisiting and extending the chronology of the sedimentary deposits inside Blombos Cave. We also map, describe and date the onshore Pleistocene geological deposits near the cave, and document and describe three seismic transects (two perpendicular to the coast and another parallel to the coast) across the Agulhas Bank. We then relate the onshore Pleistocene sequences and sedimentary deposits found within Blombos Cave to place the cave deposits within the landscape-scale chrono-stratigraphic framework developed in this study, and propose that this coarse-scale study of geogenic processes provides the broader context for finer-scale interpretations of the archaeological, sedimentary and environmental patterns revealed in Blombos Cave.

All authors have made substantial contributions to the research conducted and the writing of the paper. Jacobs wrote the paper, conducted the OSL dating of all samples and participated in both archaeological and geomorphological fieldwork. Jones led the geomorphological fieldwork and mapped and described the onshore aeolian and palaeosol sequence and conducted the mineralogical analyses. Cawthra conducted the marine geophysical survey and analyse and interpret the data and created the maps representative of different sea levels. Henshilwood is the permit holder of the site and have conducted the archaeological research over the last 2 decades. Roberts conducted the geomorphological fieldwork with Jones and Jacobs and helped with the OSL dating and interpretation of the onshore geological sequences. All authors contributed to the writing of the paper and approved the final version of the paper.

Yours sincerely,

Zenobia Jacobs

# The chronological, sedimentary and environmental context for the archaeological deposits at Blombos Cave, South Africa

Zenobia Jacobs[1,2], Brian G. Jones[3], Hayley C. Cawthra[4,5] Christopher S. Henshilwood[6,7] and Richard G. Roberts[1,2]

[1] Centre for Archaeological Science, School of Earth, Atmospheric and Life Sciences, University of Wollongong, Wollongong, New South Wales 2522, Australia.
[2] Australian Research Council (ARC) Centre of Excellence for Australian Biodiversity and Heritage, University of Wollongong, Wollongong, New South Wales 2522, Australia.
[3] GeoQuEST Research Centre, School of Earth, Atmospheric and Life Sciences, University of Wollongong, Wollongong, New South Wales 2522, Australia.
[4] Geophysics and Remote Sensing Unit, Council for Geoscience, Bellville 7535, South Africa.
[5] African Centre for Coastal Palaeoscience, Nelson Mandela University, Port Elizabeth 6031, South Africa.
[6] Evolutionary Studies Institute, University of the Witwatersrand, Johannesburg 2050, South Africa.
[7] SFF Centre for Early Sapiens Behaviour (SapienCE), University of Bergen, 5020 Bergen, Norway.

## Abstract

The site of Blombos Cave (BBC) is well known for archaeological remains that have advanced our understanding of the development of modern human behaviour during the Middle Stone Age (MSA). Occupation of the cave occurred against a backdrop of landscape-scale environmental and sedimentary processes that provide the broader context for finer-scale interpretations of the site-formation history and archaeological patterns detected in the cave deposits. Aeolian and palaeosol sequences are abundant in the vicinity of BBC and these provide a partial view of the past landscapes available to the inhabitants of the cave. An important extension to the palaeo-landscape around BBC currently lies submerged on the Agulhas Bank, as sea levels were lower than at present for the entire period of human occupation of BBC. In this paper, we revisit the optically stimulated luminescence (OSL) chronology for the full sequence of sediment deposition inside BBC, increasing the number of dated samples to a total of 40 and revising the period of MSA occupation to between 97.7 ± 7.6 and 71.0 ± 5.7 ka (uncertainties at 95.4% probability). We describe the geological successions at four main areas around BBC, estimate the time of sediment deposition using OSL, and describe and interpret three seismic profiles on the Agulhas Bank, offshore of BBC. By correlating these onshore and offshore geological sequences with the sedimentary deposits inside BBC, we place the archaeological record within a landscape-scale chrono-stratigraphic framework to examine how environmental changes may have regulated the presence or absence of humans in the cave and surrounding terrain between about 100 and 70 ka.

Key words: *optical dating*, *Bayesian age model*, *relative sea level*, *palaeo-Agulhas Plain*, *human–environment interactions*

## 1. Introduction

The south Cape coast of South Africa is home to a number of important archaeological cave sites, including Die Kelders (Marean et al., 2000), Klipdrift Shelter (Henshilwood et al., 2014), Blombos Cave (Henshilwood et al., 2001), Pinnacle Point Site 13B (Marean et al., 2010) and Pinnacle Point Site 5-6 (Smith et al., 2018) (Fig. 1). All these sites are located along the leading edges of different half-heart embayments that make them effective sediment traps. The trapped

sediments preserve an authentic record of the associated depositional processes that have also played a dominant role in shaping the stratigraphic sequences of these sites, forming the backdrop against which traces of human occupation are exposed (e.g., Karkanas et al., 2015). Since these depositional processes are landscape-scale processes, stratigraphic interpretation of the sediments inside these cave sites should be made based on geological and geomorphological knowledge of the wider landscape.

Aeolian deposits are widely preserved along the south Cape coast, often in association with palaeosols, and aeolian sand is an important component of many of the cave deposits. The timing, pace and magnitude of aeolian deposition has fluctuated, because the source of sediment is linked to the exposure of sandy coastal areas on the adjacent continental shelf as the position of the coastline has shifted due to changes in sea level (e.g., Bateman et al., 2004). Aeolian deposition could be interpreted as periods of landscape instability and change, whereas palaeosols mark breaks in dune sedimentation and only form on dunes after their colonisation and stabilisation by vegetation. Palaeosols, therefore, represent former stable land surfaces. Sand layers can be easily observed inside caves, but palaeosols rarely extend into caves, making it more difficult to recognise periods of landscape stability in cave sediment records.

Blombos Cave (BBC) is an ideal case study to investigate the relationship between the sediments found inside and outside a cave in this region. Massive aeolian and palaeosol sequences up to 50 m in height above modern sea level are preserved around BBC. The cave is situated ~100 m from the Indian Ocean shore and ~34.5 m above mean sea level (amsl), so the deposits are protected from the erosive action of storm surges and waves. It was also sealed for most of the last ~70 ka by a sand dune that covered the cliff face, became cemented and protected the site thereafter. This ensured that the Middle Stone Age (MSA) deposits were conserved in an almost pristine condition, with excellent preservation of its faunal and malacological remains.

The MSA sedimentary layers in BBC (Fig. 2) have been dated to between ~100 and 70 ka ago, placing occupation within the moderate interglacial conditions of Marine Isotope Stage (MIS) 5d to 5a and during the transition to moderate glacial conditions near the start of MIS 4 (Jones, 2001; Henshilwood et al., 2002, 2004, 2011; Jacobs et al., 2003a,b, 2006, 2013; Tribolo et al., 2006). Over this period, relative sea-level fluctuated between about –18 m to –76 m below mean sea level (bmsl) (Waelbroeck et al., 2002), exposing approximately 2.3–32.5 km of the now-submerged Agulhas Bank (Fisher et al., 2010). So, a large part of the terrestrial landscape between ~100 and 70 ka ago is now underwater, and the relationship to the onshore sedimentary records, including those trapped in BBC, is not well known. To better understand and interpret the site formation processes at BBC, and the history of human occupation and concurrent environmental changes, requires knowledge of both the onshore and offshore sedimentary records in the vicinity of the cave, the timing of changes in these records, and the correlation or interplay between them.

In this study, we revisit the chronology of the sedimentary deposits inside BBC. We map, describe and date the onshore Pleistocene geological deposits near the cave, and document and describe three seismic transects (two perpendicular to the coast and another parallel to the coast) across the Agulhas Bank. We then relate the onshore Pleistocene sequences and sedimentary deposits found within BBC to place the cave deposits within the landscape-scale chrono-stratigraphic framework developed in this study. Linking these two records can shed light on how long-term environmental and landscape changes may have regulated the absence and presence of humans in the cave and surrounding terrain. We interpret the environmental proxy records in relation to the new knowledge gained from exploration of the offshore records.

We propose that this coarse-scale study of geogenic processes provides the broader context for finer-scale interpretations of the archaeological, sedimentary and environmental patterns revealed in BBC.

## 2. Setting

BBC is well known as an important site for understanding the MSA, and specifically the development of symbolic behaviour among *Homo sapiens* (Henshilwood et al., 2001a,b, 2002, 2004, 2011, 2018; Henshilwood and Dubreuil, 2011; d'Errico et al., 2001, 2005; Mourre et al., 2010; Vanhaeren et al., 2013). The cave is situated approximately 300 km east of Cape Town and just west of the village of Still Bay (34°25'S, 21°13'E; Fig. 1), bounded by the Duiwenhoks River to the west and by the Goukou River to the east. The coastal forelands around BBC are dotted with massive aeolianite and palaeosol outcrops sitting atop the Table Mountain Group sandstone basement. The modern shoreline is rocky, with the adjacent habitat dominated by fynbos vegetation that hosts faunal communities adapted to scrubland environments. The small animals include the rock hyrax, Cape dune mole rate, tortoise and small browsing bovids, including the Cape grysbok and klipspringer and the larger Cape bushbuck. Fluctuations in sea level and variations in site-to-shoreline distances during MSA occupation of BBC would have affected the availability of habitable land and changes in the broader environment (Compton, 2011).

Roberts et al. (2008) provide the only published investigation that dated aeolianite and palaeosol sequences near BBC. They studied a well-exposed, 55 m-thick succession of predominantly aeolian deposits located ~30 km to the east of BBC. Elephant and giraffe trackways are preserved in the sediments deposited at ~140 ka (Helm et al., 2018), but most of the succession accumulated between 126 ± 7 and 91 ± 5 ka, with soil horizons formed near the start and end of this time interval. A major break in sedimentation separates the latter palaeosol and the Holocene aeolian deposits.

The MSA deposits inside BBC also provide a glimpse into what the environments might have looked like at different times, and how humans may have adapted to changes in landscape and ecology. Evidence in the form of macrofauna (Henshilwood et al., 2001a; Thompson and Henshilwood, 2011; Reynard et al., 2014; Discamps and Henshilwood, 2015; Badenhorst et al., 2016; Reynard and Henshilwood, 2017, 2018a,b), microfauna (Hillestad-Nel and Henshilwood, 2016), shellfish (Henshilwood et al., 2001a; Roberts et al., 2016), terrestrial snail shells (Langejans et al., 2012), ostrich eggshells (Roberts et al., 2016) and reptiles (Thompson and Henshilwood, 2014a,b) occur in a number of discrete layers throughout the sequence. These layers have been lumped together into four phases: M3 (layers CPA–CH), M2 lower (layers GCAC–CGAA), M2 upper (layers CFD–CF) and M1 (layers CD–CA) (Fig. 2B). A culturally-sterile layer of undisturbed sand (DUN) overlies the MSA sequence and separates it clearly from the Later Stone Age (LSA) deposits. All layers consist primarily of sand, with lenses or stringers of shells, organic matter and ash. Some layers are dominated by shell that forms thicker clast-supported lenses (e.g., layer CI), and combustion features occur frequently throughout the deposit.

Overall, the various lines of proxy evidence paint a picture of relatively stable environmental conditions during phase M3, with gradual changes starting to occur towards the end of M3 and through M2, with M1 representing a period of accelerated change. Large ungulates became more dominant compared to small browsers in phase M1, suggesting a shift from scrubland vegetation to more open grassland (Henshilwood et al., 2001a; Thompson and Henshilwood, 2011; Discamps and Henshilwood, 2015). A similar change is suggested by shifts in the micromammal communities (Hillestad-Nel and Henshilwood, 2016). *Donax serra* shellfish

appears for the first time in phase M1, suggesting the presence of sandy beaches in the area (Henshilwood et al., 2001a). Oxygen and carbon isotope measurements on ostrich eggshell suggest a shift from greater humidity and winter rainfall conditions to increasing aridity during M1, associated with a change in year-round rainfall or the presence of aridity-linked Crassulacean acid metabolism (CAM) vegetation (Roberts et al., 2016).

## 3. Methods

### *3.1 Optically stimulated luminescence (OSL) dating*

We used OSL dating to obtain burial ages for sediments inside and outside the cave (Huntley et al., 1985; Aitken, 1998; Duller, 2004; Wintle, 2014; Roberts et al., 2015). Fifteen new samples were collected from inside BBC; nine from phase M3, three from sand layers immediately preceding M3, and three from a small chamber at the back of the cave that was infilled with sediment (Figs 2E and 2F). Samples inside the main cave are listed by layer and excavation square in Table 1 and can be related to the cave plan map and stratigraphy in Figs 2A and 2B, respectively. We also collected 12 samples from the onshore Pleistocene deposits at three outcrops located between 1.2 km northwest and 250 m west of BBC (Fig. 3). Equivalent dose ($D_e$) values and environmental dose rates were estimated using the methods, equipment and procedures described and tested previously for samples from BBC (Jacobs et al., 2003a,b, 2006, 2013). Some updates and checks were required for error calculation of OSL measurements and beta dose rates (Jacobs and Roberts, 2015, 2017; Li et al., 2017). Individual $D_e$ values for each sample were combined using the central age model of Galbraith et al. (1999). Using the approach presented in Li et al. (2016) and Hu et al. (2019), we also tested whether samples with $D_e$ values close to the saturation level of the dose response curve had truncated $D_e$ distributions that would, therefore, underestimate the true $D_e$. We recalculated, where possible, the $D_e$ values and dose rates published previously for all BBC samples to ensure comparability between all age estimates in order to place them on a common timeline.

### *3.2 Onshore field mapping, mineralogy and lithology*

Onshore stratigraphic sections were measured and described, and samples were collected for OSL dating. Horizontal and vertical coordinates for all field samples were obtained using a hand-held GPS, while the four main stratigraphic profiles outside the cave (Fig. 5) were surveyed using a theodolite. The logging of geological sections and field descriptions followed standard procedures and facies were determined according to primary sedimentary structures. Mineralogy was investigated using thin sections and X-ray diffraction (Phillips 1150 PW Braggs-Brentano diffractometer, with 1 kW CuKα radiation and GBC SIE122 data acquisition software). Grain size was determined from visual comparison charts, augmented with thin-section analysis and laser particle-size measurements (Malvern Mastersizer 2000).

### *3.3 Offshore field mapping*

The seafloor in front of BBC was mapped over three high-resolution, single channel, reflection seismic surveys, with data coverage extending from the Breede River in the west to Plettenberg Bay in the east (Cawthra et al., this issue). First, a pinger sub-bottom profiling survey was carried out from Knysna to Still Bay using a GeoAcoustics 5430A transmitter, an Octopus 760 seismic processor and an over-the-side mounted array of four Massa transducers. The second seismic voyage was a Parasound survey, conducted on R.V. Meteor cruise M123 (Zabel et al., 2017). The parasound echosounder (Atlas Hydrographics) operated on two frequencies (18 and

22 kHz), with the sound beams emitted from hull-mounted transducers. All systems were configured to acquire digitised SEG-Y data. Processing methods are described in Cawthra et al. (this issue) and time-depth data were extrapolated to surface units to produce a geological map for the Last Glacial Maximum (~21 ka).

Sediment grab sampling and scuba diving surveys in Mossel Bay enabled seafloor surface outcrops to be sampled (details in Cawthra et al., 2018) and extrapolated along strike towards the west. A total of six marine vibracores were taken over two marine expeditions in ancient river valleys and lagoons from the R.V. Meteor, with promising spots identified from the sub-bottom profiling surveys. Details of these sampling campaigns are given in Ekau et al. (2014), Cawthra et al. (2016), Hahn et al. (2017) and Zabel et al. (2017).

## 4. Results

### *4.1 Chronological framework for sediment deposition inside BBC*

All published age estimates from a number of studies are summarised in Roberts et al. (2016: Table S1). The final OSL ages from the present study are listed in Table 1, together with the supporting $D_e$ and dose rate estimates. Uncertainties on the ages are given at 1σ (the standard error on the mean) and were estimated by combining, in quadrature, all known and estimated sources of random and systematic error. Ages are presented in stratigraphic order, although the order of samples within a layer is arbitrary, as the relative positions of samples between the different squares and profiles are not known. The ages reported here supersede those published previously.

All new ages for sediment samples from the main cave are from phase M3 (Fig. 2B) and from the sand layers preceding M3, which we refer to in this paper as 'pre-M3'. The latter is represented by massive sands that are unconsolidated in places and cemented in others, forming a solid block of hard ground devoid of any archaeological remains (Fig. 2C). Three samples from the pre-M3 phase gave statistically consistent ages of 101 ± 6, 100 ± 8 and 110 ± 5 ka (Table 1), which are similar to the five ages obtained for the lowermost layers of phase M3 (layers CP and CPA). The 13 samples from layers CO to CI in phase M3 yielded ages ranging from 95 ± 5 ka (BBC08-7) to 83 ± 4 ka (BBC08-12). These ages are not in stratigraphic order but are statistically consistent (i.e., the ages are compatible with the estimated uncertainties and represent a random sample from within this time interval). Layer CH, at the top of phase M3, is systematically younger than the rest of M3, with ages of 82 ± 5 ka and 77 ± 7 ka. These ages differ from those presented in Henshilwood et al. (2011), who suggested a shorter duration for M3 (101 ± 4 to 94 ± 3 ka), mostly because that study used the finite mixture model for $D_e$ determination, which involves alternative assumptions.

The sediment sequence in the rear chamber of BBC can be divided into 5 broad units (Fig. 2F). Unit A at the base (which was defined arbitrarily and not because bedrock was encountered) is a ~5 cm-thick green banded quartz-illite-kaolinite deposit indicative of past waterlogging. This is overlain by a very moist and well-sorted ~25 cm-thick dark red/brown silty sand (Unit B), for which an OSL age of 128 ± 17 ka (BBC10-11) was obtained. No deposit of equivalent age has been found inside the main cave. A 5 cm-thick layer of cobble-size bedrock clasts separates Units B and C, the latter consisting of a ~10 cm-thick well-sorted dark brown medium sand with abundant heavy minerals. This, in turn, is overlain by a ~40 cm-thick block of calcarenite, which is either a fallen slab or part of the bedrock extending into the sediment. Unit D is a ~60 cm-thick well-sorted olive green/yellow medium sand with no obvious sedimentary structure; it is likely wind-blown material redeposited by water inside the cave. Sample BBC10-10 was collected from Unit D and gave an age of 99 ± 5 ka, consistent with the ages of the pre-M3

samples and the sandy base of phase M3. Unit E is ~45 cm-thick inhomogeneous red/brown medium-coarse sand with abundant stone and shell clasts that appears to have been water-lain. MSA artefacts were found in this unit that possibly slumped into this rear chamber. The age of 87 ± 6 ka obtained for this layer (BBC10-9) is consistent with occupation during phase M3. A small air space separates the top of Unit E from the low and sloping bedrock ceiling.

All single-grain OSL ages from the main cave were included in a Bayesian statistical model on the OxCal platform (OxCal 4.2.4) (Bronk Ramsey, 2009a; Bronk Ramsey and Lee, 2013). Only the unshared errors were included in the model (Rhodes et al., 2003); these are shown in brackets in Table 1. We used the sequence of the six stratigraphic phases (pre-M3, M3, M2 lower, M2 upper, M1 and DUN) as prior information. Each of the stratigraphic phases was modelled as a *Phase*, in which the measured ages are assumed to be unordered and uniformly distributed. A transitional *Boundary* was placed between each *Phase*, assuming that the BBC sediments have accumulated continuously without any significant breaks. The modelled probability distributions of these *Boundaries* constrain the start and end ages of consecutive *Phases*, which were arranged into a *Sequence* under the assumption that the stratigraphically lowest *Phase* is older than those above. A general t-type outlier model (Bronk Ramsey, 2009b) was used to assess the likelihood of each age being consistent with the fitted model. Each age was assigned an outlier probability of 5%.

The Bayesian modelled OSL chronology for BBC is presented in Fig. 4, and the corresponding data are provided in Table 2. Thirty-seven samples were included in the Bayesian age model. The modelled ages are reported with uncertainties at the 95.4% confidence interval; the first uncertainty is the total unshared-only error and the second is the total uncertainty, which also includes the shared errors. Deposition of sand in BBC occurred from at least as early as the last interglacial period, with the oldest sand in the rear chamber deposited 128 ± (17, 16) ka ago. The sand at the base of the current excavation of the pre-M3 phase started to accumulate 107.8 ± (10.3, 12.1) ka ago. Transition to first human occupation of the site occurred at 97.7 ± (4.9, 7.6) ka, followed by M2 lower at 82.5 ± (3.8, 6.2) ka, M2 upper at 76.0 ± (3.3, 5.6) ka, and M1 at 73.7 ± (2.6, 5.2) ka. The MSA deposits ceased accumulating at 71.0 ± (3.8, 5.7) ka, after which a dune sealed the cave until the late Holocene. This updated and extended chronology for BBC indicates that sediment deposition occurred from MIS 5e through to MIS 4, with human occupation restricted to MIS 5d–5a.

### *4.2 Stratigraphic successions of onshore sedimentary outcrops outside BBC*

Schematic representations of the geological successions observed in the field at four locations are presented in Fig. 5. The 12 stratigraphic units (Units A–L) are described below. Most of the Pleistocene Waenhuiskrans Formation units were sampled for OSL dating to create a chronological framework for sediment deposition outside BBC.

#### Unit A: Basement

The escarpment and cave-forming succession at Blombos has been protected from wave erosion by strongly deformed and folded quartz-rich Ordovician sandstone outcrops of the Table Mountain Group. In many areas, the dips in these Ordovician strata are almost vertical and small patches of tight, small-scale chevron folding were recorded. The Table Mountain Group is unconformably overlain along a very irregular surface by the Cenozoic Bredasdorp Group. This is represented by patches of the De Hoopvlei Formation (shelly conglomerate and marine sands), followed by the much thicker calcareous aeolian sands of the Pliocene Wankoe Formation, which forms most of the coastal escarpment. The escarpment reaches a height of

100–120 m and is capped, and partly coated, by Pleistocene (Waenhuiskrans Formation) and Holocene (Strandveld Formation) aeolian sand. At the base of the cliff, the Table Mountain sandstone forms an irregular wave-cut coastal platform at heights of 0–17 m amsl. In the vicinity of BBC, aeolian deposits have been stripped from the side of the sandstone escarpment up to a height of ~60 m, exposing the entrance to BBC (~34.5 m amsl) and a larger cave ~50 m to the northeast (~42 m amsl).

Unit B: Lower, thinly-bedded marine sands

Unconformably above a higher exposure of the Table Mountain Group, on a headland ~1.2 km west of BBC, lies a distinctive 4–5 m-thick marine sandstone unit characterised by flat and small-scale cross-bedding (Fig. 6A). The basal part of the sequence consists of small trough (to 20 cm-thick) and planar (<1 m-thick) cross-bed sets interbedded with flat and low-angle laminated beds. A few lensoidal (to 20 cm-thick) massive beds are also present. Material consists of yellow-brown medium- and coarse-grained shelly sand with darker brown surface coating. The coarser grains are mainly shell fragments; acid treatment to disaggregate the grains yielded a mean grain size in the fine-sand range (Table 3). The dominant palaeocurrent trend in this succession is onshore to 335°, but a minor secondary trend is towards 122°. A few infilled solution pipes indicate a period of dissolution prior to deposition of the overlying succession. OSL sample BBC10-G6 was collected from ~17.7 m amsl, near the exposed base of this unit (34°24.645'S, 21°12.583'E; Fig. 6A).

Unit C: Lowest dune sands

Cross-bedded moderately cemented sandstone is exposed in a road cutting 1 km east of BBC (~27 m amsl at 34°24.985'S, 21°13.989'E). A palaeosol at the base of this exposure consists of massive fine- to medium-grained sandstone with numerous small, calcite-cemented nodules near the top (Fig. 7A). It is abruptly overlain by a large aeolian dune up to 3–4 m high, interspersed with thin, flat-bedded sandy and silty interdune successions. Average palaeocurrent trend for these large dunes is towards ~140°. A large footprint is preserved in the finer and more thinly laminated lower part of a dune that overlies a scour or reactivation surface (Fig. 7B). No OSL samples were collected from this unit, so the age and stratigraphic unit to which this aeolian sequence belongs is uncertain, but it represents part of the Waenhuiskrans Formation that pre-dates the main dune succession around BBC.

Unit D: Dune unit below Palaeosol A

The succession beneath Palaeosol A infills irregularities along the coast, as it unconformably overlies the Table Mountain Group and onlaps the two earlier sandstone units. It ranges in thickness from 4 m to 25 m. The top of the unit is gently undulating on a broad scale, and forms a distinctly mappable unit extending at least 1.3 km west and 700 m east of BBC (to 34°24.997'S, 21°13.651'E).

Near the unconformity surface at lower elevations, the cross-beds are 1–2 m thick (Fig. 7C), show a more erratic palaeocurrent trend (000-080°), and tend to consist of medium- to very coarse-grained sand. The coarsest fragments generally consist of platy shell fragments (Fig. 7D). Minor flat bedding is also present in the lower part of this unit and may represent storm or sheetwash deposits. The upper part of the succession consists of more uniform, large-scale cross-bedded medium-grained sandstone of aeolian character (Fig. 7E) with a general palaeowind direction towards ~135°, although some cross-beds have truncated the regular dunes and show up to 40° divergence in palaeowind trend (Fig. 7F). Many of the cross-beds are 4–6 m thick and consist of yellow-brown medium-grained sandstone with the quantity of shell

fragments decreasing in size and abundance at higher elevations. Some of the dunes show reactivation surfaces, indicating variable wind orientation and strength.

The OSL sample from this succession (BBC10-G10) is from a large cross-bed in the upper third of the unit (~16 m amsl at 34°24.788'S, 21°12.996'E), ~120 m southeast of BBC10-G8 (Fig. 8B). The sandstone at the BBC10-G10 location is orange-brown and contains no shells or large shell fragments, but it does contain small sand-sized shell fragments. East of BBC, beneath Palaeosol A at 34°24.938'S, 21°13.526'E, a planar cross-bedded medium- to coarse-grained sandstone shows a palaeowind trend towards 140°.

Unit E: Palaeosol A

Palaeosol A forms a distinctive, continuous marker unit in the area west of BBC, and it can also be traced discontinuously to the east of the cave. It directly overlies large-scale dune cross-bedding, but has a fairly flat base. It generally ranges from 30 cm to 1 m in thickness, but reaches a maximum thickness of 2.4 m over a few basal hollows (Fig. 8A). Thus, it has an average thickness of ~1 m but is lensoidal, showing gentle lateral thickening and thinning. Palaeosol A predominantly consists of light brown massive structureless fine- to medium-grained silty sand (Fig. 8B). The sand content (80–90%) has a mean grain size of ~350 μm (Table 3). This palaeosol commonly contains scattered land snails, including *Achatina zebra*, common *Tropidophora ligata* and rare *Trachycyctis capensis*. It also contains scattered small shell fragments (probably of land snails). Rhizomorphs are present in places at the top of the underlying dune sandstone beds, but are more common in a 10–15 cm-deep zone at the top of the unit (Fig. 8C). The rhizomorphs are carbonate-cemented and stand out during modern weathering of the ancient soil. OSL sample BBC10-G1 was collected from the lower part of the 2.4 m-thick palaeosol (~24.5 m amsl at 34º 24.868'S/21º 13.163'E; Fig. 8C), in a protected enclave 150–300 m west of BBC, where the thick soil succession has accumulated with no intervening dune deposits.

Farther west, Palaeosol A is thinner and is sandwiched between the underlying and overlying cross-bedded dune sand deposits (Fig. 8B). The palaeosol is a slightly darker orange brown colour at this location, but the soil characteristics are the same and include scattered fragments of land snails (*A. zebra* and common *T. ligata*). OSL sample BBC10-G8 was taken from the upper part of the 1.5 m-thick palaeosol (~24 m amsl at 34°24.739'S, 21°12.935'E; Fig. 8B). The latter thins in both directions away from the collection site, with rhizomorphs present on either side but not where the OSL sample was taken. A siliceous MSA flake was seen at the same level as BBC10-G8, but 1.15 m to the northwest.

East of BBC (at 34°24.938'S, 21°13.526'E), Palaeosol A is ~0.5 m-thick and contains common *T. ligata*. It is overlain by ~3 m of Unit F dune sand before being covered by the youngest dune succession (Unit K).

Unit F: Between Palaeosols A and B

In the interdune area, ~200 m west of BBC, Palaeosol B overlies Palaeosol A with only ~2 m of structureless sand separating the two soil units (Fig. 8C). Farther west, Palaeosol A is directly overlain by large-scale planar dune cross-beds with a total thickness of up to 6–8 m (Figs 8B and 9A). A second dune, lensoidal in shape and up to 4 m thick, cuts across the lowest dune. It consists of medium- to coarse-grained, slightly shelly sand and shows several reactivation surfaces. OSL sample BBC10-G9 (~28 m amsl at 34°24.735'S, 21°12.943'E; Fig. 9A) is from near the base of this upper dune. The mean grain size of these dunes is ~440 μm (Table 3) with

a mean palaeowind direction towards 050°, but the reactivation surfaces indicate variable palaeowind strengths.

The upper part of the same unit, ~1.3 km west of BBC, shows a large planar cross-bed dipping onshore (palaeowind direction ~040º) (Fig. 9B). A block of sandstone from this cross-bed (sample BBC10-G7 from ~31 m amsl at 34°24.577'S, 21°12.569'E) was collected for OSL dating. It consists of buff to yellow-brown medium- to coarse-grained sandstone with numerous small shell fragments. This represents the coarsest analysed sand, with a mean grain size of ~660 μm (Table 3). Some reactivation surfaces within the dune show lower dips. The dune is weakly cemented in its lower part, but has stronger carbonate cement at the top, capped by calcrete.

Unit G: Palaeosol B

In the multi-soil area, 150–300 m west of BBC (Fig. 8A), Palaeosol B was sampled ~4 m above Palaeosol A (Figs 8C and 9D). It consists of medium-grained (~435 μm; Table 3) silty sandstone with a few scattered complete and fragmented shells of land snails, including *A. zebra* and numerous smaller *T. ligata* and rare *T. capensis*. The palaeosol is ~2.5 m thick and overlies a zone of poor outcrop consisting of massive sandstone. It also contains a few small rock and calcrete fragments. Rhizomorphs are common in the upper part of the soil profile. OSL sample BBC10-G2 (from ~30 m amsl at 34°24.865'S, 21°13.182'E) was collected from ~2 m below the rhizomorph zone (Fig. 9D).

West of the multi-soil area, Palaeosol B overlies a planar surface at the top of the cross-bedded sandstone (Fig. 9A) above Palaeosol A. The vertical separation between the palaeosols increases here to about 6–8 m. Palaeosol B, which is ~2 m thick, contains numerous rhizomorphs towards the top of the horizon, with a few rhizomorphs extending into the underlying dune (Fig. 9A).

Unit H: Between Palaeosols B and C

In the multi-soil area, 150–300 m west of BBC (Fig. 8A), Palaeosol B is overlain by a thin massive sandstone that grades upwards into Palaeosol C (Fig. 9C). In contrast, in the area 500–800 m west of BBC, Palaeosol B is overlain by additional planar cross-bedded medium-grained yellow-brown sandstone sets, up to an exposed total thickness of about 6–7 m. These dunes show minor changes in wind direction, with a mean wind direction of ~075°.

Unit I: Palaeosol C

Palaeosol C consists of fine- to medium-grained pinkish brown silty sandstone (Figs 9C and 9E). It is ~2 m thick and overlies 2–3 m of apparently massive sandstone. OSL sample BBC10-G3 was taken from ~34 m amsl at 34°24.875'S, 21°13.168'E. The sandstone contains scattered, larger (to 4 mm) fragments of shell (probably land snails) and rare calcrete clasts. It also contains a few scattered high-spired gastropods, while the equivalent unit ~50 m farther west also contains *A. zebra* and smaller *T. ligata*. Large rhizomorphs are common in the upper 40 cm, but root traces extend down in a few places for 1 m or more.

Unit J: Above Palaeosol C

OSL samples BBC10-G4(2) (~40 m amsl) and BBC10-G4 (~42 m amsl), both at 34°24.846'S, 21°13.158'E, are from a sequence of soils below the top dune that were only seen in the multi-soil area (Fig. 9F). At the base of this sequence, a thin massive sand shows a sharp bedding

contact with Palaeosol C (Fig. 9E). It is overlain by another thin soil and a further massive sand with rhizomorphs at the top. This is overlain, in turn, by a poorly consolidated fine- to medium-grained yellow-brown aeolian dune sand, from which BBC10-G4(2) was collected. In places, this dune grades up into soil with rhizomorphs and a thin calcrete cap. This dune is erosionally truncated and overlain by medium- to coarse-grained sandstone showing evidence of sub-horizontal bedding. The latter may represent sheetwash deposits (BBC10-G4), with coarse laminae, often overlying shallow scour surfaces, representing more energetic storm events. This unit contains two 40 cm-thick layers with rhizomorphs at the top, a few *T. ligata*, and is overlain in places by very thin calcrete.

Unit K: Top Dune

Most of the older units are partially covered by a very large-scale dune cross-bed that appears to have advanced over the top of the escarpment, forming a large angle-of-repose dune draped across the older land surface. It is the youngest identifiable unit in the Waenhuiskrans Formation (Figs 7G and 7H). The base of this unit is very irregular and unconformably covers the partially eroded surface of the older dune and soil sequences, which can be seen to rise landwards where gullies have cut through the younger dune. The latter consists of medium- to coarse-grained (275–615 μm; Table 3) shelly sand, probably blown onto the top of the ridge from the beach farther west. Some of the avalanche sets are up to 20–30 cm thick, but most are much thinner. The trend of this dune varies from 160 to 210° and it appears to form two large arcuate masses, one on either side of BBC and the multi-soil area. OSL sample BBC10-G11 was collected from about one quarter of the way up the visible dune slope, but only ~1 m vertically above the base of the dune (~30 m amsl at 34°24.781'S, 21°13.026'E).

Just outside BBC, remnants of the top dune sequence are cemented with calcite and were previously sampled and dated (ZB13) by Jacobs et al. (2003a,b). East of BBC (at 34°24.938'S, 21°13.526'E), the top dune overlies Palaeosol A and ~3 m of Unit F, and shows a palaeowind trend towards 210°.

At the eastern end of the study area, the top dune directly overlies the lower marine sands and is indurated with calcite cement beneath a flowstone calcrete capping (OSL sample BBC10-G5, ~25 m amsl at 34°24.643'S, 21°12.603'E). This top dune unit shows planar cross-beds of moderate size, with an eastward palaeowind direction (~075°; Fig. 6B), interspersed with minor low-angle or flat bedding.

Unit L: Calcrete

Weakly to moderately developed flowstone calcrete covers most of the older strata 1.2–1.3 km west of BBC. Many calcrete and calcite-cemented sandstone clasts are incorporated on its upper surface. The flowstone represents a slope-wash deposit that extends down partly over older aeolian cross-beds at the edge of the cliff and post-dates the development of a few infilled solution pipes in the older Unit B sequence. Minor penetrative calcrete is also present, especially extending down rhizomorphs and small dissolution cavities into the underlying aeolian sands. Other small patches of calcrete occur overlying various earlier successions, including the top dune.

*4.3 Mineralogy*

The lower, thinly-bedded marine sand (Unit B) differs from the overlying units in having a higher K-feldspar content (Table 3), but the carbonate content could not be assessed because

the sample had been acid-leached during preparation for OSL dating. Samples from the lower dunes that had not been acid-leached contain a variable content of carbonate (20–48% by weight), mainly in the form of shell fragments. They contain minor plagioclase (2–3%) and are dominated by quartz (48–73%). The associated soils have a similar composition, but are characterised by lower carbonate contents and higher clay contents – probably a function of carbonate leaching during soil development. The top dune is very calcareous, with similar amounts of quartz and calcite, indicating a large quantity of shell detritus, some of which has been remobilised to form cement. Leaching of carbonate from these upper dune sands is probably responsible for the formation of calcrete caps in other parts of the sequence.

### *4.4 Chronological framework for sediment deposition outside BBC*

Twelve multi-grain OSL ages were obtained for three sedimentary facies (aeolian dunes, marine sands and palaeosols) from three main areas around BBC (Figs 3 and 5). The ages and supporting data are presented in Table 4.

The earliest dated sediment in the succession is the thinly-bedded marine sand (Unit B) lying above a higher part of the Table Mountain Group (~16 m amsl), collected from the headland ~1.25 km west of BBC (Figs 3 and 6A). This sample (BBC10-G6) gave an age of 386 ± 57 ka, suggesting deposition during MIS 11. This is consistent with MIS 11 marine deposits farther to the east of BBC, at Klein Brak River, Dana Bay and Hartenbos River, which have been dated to 391 ± 16, 388 ± 14 and 370 ± 18 ka, respectively (Jacobs et al., 2011; Roberts et al., 2012). At Klein Brak River, a maximum MIS 11 sea level of 13 ± 2 m above mean low tide (amlt) was calculated at the contact between the shoreface and foreshore facies (Roberts et al., 2012). At Dana Bay, the MIS 11 deposits were in some places truncated by deposits dated to MIS 5e, but the preferential preservation of this thinly-bedded succession on this elevated part of the coast is probably because it lies well above the maximum MIS 5e high-stand (6.2 m amlt) in southern Africa (Carr et al., 2010; Roberts et al., 2012). Elsewhere along the south Cape coast, where the elevation of the Table Mountain Group is lower, these earlier successions would have been eroded during MIS 5e.

Sea level fell ~45 m after the MIS 5e high-stand, exposing coastal sands that could be moved eastwards along the coast and accumulate as a series of moderate-size parabolic dunes adjacent to the exposed Table Mountain Group cliffs. The undated aeolian succession (Unit C; Figs 7A and 7B), 1 km east of BBC, lies below the main Blombos dune succession and is likely part of a MIS 5e sequence. It starts with a poorly exposed palaeosol, which is overlain by a layer with abundant calcrete fragments, possibly concentrated by wind ablation. This is overlain by large, tabular aeolian cross-beds that show an eastward palaeo-wind trend. This sequence is very similar, and possibly equivalent, to the MIS 5e succession of palaeosol and aeolian deposits at Still Bay, 30 km east of BBC, which have been dated to 121 ± 7 and 114 ± 7 ka, respectively (Roberts et al., 2008).

Unit D, the large aeolian unit that underlies the first of the palaeosols in the study area (Figs 7C–F and 8A), accumulated 104 ± 7 ka ago, consistent with deposition during MIS 5d. The succession of multiple dune cross-beds and soil profiles yielded ages of 91 ± 4 ka (Unit E), 92 ± 6 ka (Unit F), 91 ± 6 ka (Unit G) and 87 ± 7 ka (Unit I), all of which are consistent with deposition during MIS 5c. These sedimentary units are equivalent in age to the uppermost palaeosol in the Still Bay section, dated to 91 ± 5 ka (Roberts et al., 2008).

Unit J is a complex series of dune, palaeosol and sheetwash deposits identified only in the multi-soil area (Fig. 5). The top part of this succession yielded ages of 83 ± 6 and 79 ± 6 ka, suggesting deposition during the latter part of MIS 5b and the start of MIS 5a. The large angle-of-repose

dunes (Unit K), which are draped across the partially eroded MIS 5 succession and likely sealed BBC, are dated to 72 ± 4 ka, consistent with deposition at the transition from MIS 5a to MIS 4.

The three main periods of dune accumulation recorded in the Blombos area correspond to the three younger periods of extensive aeolian deposition recorded by Bateman et al. (2004) in two other parts of the south Cape coast (110–140 km west and 170 km east of BBC).

### *4.5 Transects across the Agulhas Bank*

Three seismic transects, two oriented perpendicular (Fig. 10A and 10B) and one parallel (Fig. 10C) to the shore, bracket the location of BBC. The two perpendicular transects extend to 48 km and 34 km offshore, with maximum water depths of ~75 m and ~80 m, respectively. These transects demonstrate acoustic facies that have been sampled and verified in selected locations along the south Cape coast (Cawthra et al., 2016). The transect profiles are dominated by acoustically-impenetrable material interspersed by semi-transparent deposits preserved in pockets in swales between ridges. Shelf sands (yellow in Fig. 10) are preserved in patches across the shelf and have a transparent seismic signature. The inner shelf is not mapped on these profiles, but the terrace that separates it from the mid-shelf (the landward edge of the profile) is covered by shelf sands and underlain by acoustically-impenetrable material, which we interpret as aeolianite. This aeolianite unit (orange) is widespread and interspersed with a seismically semi-transparent unit composed of lagoonal deposits (blue). Also identified are floodplain deposits (green) associated with the Breede, Duiwenhoks and Goukou Rivers that created deeply incised channels on the Agulhas Bank (grey).

These transects have been integrated with geological and sedimentological datasets to produce a Last Glacial Maximum geological map for the Agulhas Bank that serves as a suitable 'average Pleistocene glacial' scenario (Cawthra et al., this issue). Here we use this as a base map to show the surficial geology of the exposed shelf at three different mean sea levels (Fig. 11): –50 m below mean sea level (bmsl), which is representative of the lowest sea level prior to and during the M3, M2 lower and M2 upper phases of BBC occupation (Fig. 11A); –60 m bmsl, the average sea level for the relatively short M1 occupation phase (Fig. 11B); and –72 m bmsl, the average sea level at the end of cave occupation and during deposition of the dune sand (Unit K) that sealed BBC (Fig. 11C).

Placement of the –50 m bmsl shoreline position on this map (Fig. 11A) shows that the coast lay only ~3.5 km from BBC. This is at the shorter end of the range of modelled distances proposed by Fisher et al. (2010), who estimated an average distance from BBC to the coastline of 7.35 km (range = 2.33–9.42 km). Offshore and almost adjacent to the cave, the bedrock substrate is composed of silty mudstone and sandstone containing subordinate shale of the Lower Cretaceous Uitenhage Group Kirkwood Formation (orange in Fig. 11). Floodplain sediments, including deposits laid down in an estuarine environment, outcrop within 6 km to the west of BBC and are associated with the now-submerged extension of the Duiwenhoks River (stippled pale yellow). About 6 km east of BBC, Table Mountain Group sandstones outcrop on the modern shore and extend onto the inner shelf (purple). At –50 m bmsl, the coastline was associated with a cordon of calcareous coastal dunes (yellow), extending eastwards from the mouth of the Duiwenhoks River and terminating on the eastern margin of the Still Bay embayment (Fig. 11A).

Placement of the –60 m bmsl shoreline on the map (Fig. 11B) shows that the coast lay ~5.7 km from BBC. This is shorter than the average modelled distance from BBC to the coastline of ~12.9 km (range = 5.9–32.3 km). Similar types of rocks and sands outcrop at this depth. At this time (contemporaneous with the final phase of BBC occupation), the Breede and Duiwenhoks

Rivers flowed eastwards, with their respective floodplains within ~21 and ~4 km from BBC. The mouth of the Duiwenhoks River and its associated estuary were ~4.8 km from BBC. The coastline was dominated by the large mouths of the three main rivers and their estuaries, which were connected with either calcareous dune cordons or mudstone and sandstone of the Kirkwood Formation.

Placement of the –72 m bmsl shoreline on the base map (Fig. 11C) shows that the coast was situated 16–30 km from BBC, with the shortest site-to-shoreline distance in a south–southwest direction. Geological features extending onto the middle shelf (terminology after Cawthra et al., 2016) indicate a greatly expanded coastal plain. The Kirkwood Formation is overlain by the Buffelskloof Formation along this part of the coast, and the contact separating these units trends southwest–northeast on the mid-shelf offshore of BBC. The Buffelskloof Formation is draped by a veneer of terrestrial mud on either side of the Duiwenhoks and Goukou Rivers. Cawthra et al. (this issue) propose that the associated soil is a deep and highly fertile clay with neutral pH. Less than 25 km from BBC, sand dunes extended up to 14 km inland from the –72 m shoreline, with back-barrier lagoons and a substantial cobble surface exposed in deflated areas.

## 5. Discussion

Figure 12 is a schematic representation of the stratigraphic sequences inside and outside BBC (not drawn to scale), with notional chronological correlations indicated by the broken lines between the two stratigraphic columns. In the following discussion, subdivided into five broad time periods, we relate the MSA occupation history of BBC to the wider environmental context.

### *5.1 Pre-occupation and initial occupation (phase M3)*

The oldest deposit in BBC is found only inside the small chamber at the back of the cave (Figs 2D to 2F) and is thought to be associated with the undated Unit C (dune sands), which was likely deposited immediately after the MIS 5e high-stand (Figs 8A and 8B). No MIS 5e beach deposits are preserved in the vicinity of BBC, perhaps due to the predominantly rocky coastline.

The sandy pre-M3 and initial M3 (layers CPA and CP) phases can be correlated to Unit D (dune sands), which were all deposited during the MIS 5d sea-level transgression from about –45 to –21 m bmsl. The lower part of Unit D is coarser grained than the overlying dune sands, with thinner cross-beds preserved due to later dune erosion. Some of the dunes are separated by horizontal stratification that may represent sheetwash. The *in situ* formation of calcrete in the BBC pre-M3 deposits (Fig. 2C) suggests that these sands were near the surface for some time, with sufficient calcium carbonate and moisture available to become cemented, perhaps through capillary action. The first archaeological evidence appears in layer CP, including ochre tool kits contained in *Haliotis midae* shells (Henshilwood et al., 2011) and a small but heterogeneous stone tool assemblage suggestive of transient occupation of the site at this time (Douze et al., 2015). No detailed information has been published on the environmental proxy evidence from these layers.

### *5.2 Subsequent occupation during phase M3*

Most of the rest of the M3 phase (layers CO–CI) has ages that are statistically consistent with each other and with the ages for Units D–I outside BBC. The latter units represent the large multi-soil and interdune sequences that dominate the landscape today (Fig. 8). Deposition occurred during MIS 5c (96–88 ka) and MIS 5b (87–82 ka), so these dunes and palaeosols

formed when sea level was between about –49 and –42 m bmsl. The coastline was ~3.5 km away from BBC at lowest sea level exposing predominantly Mesozoic mudstone and siltstone (Fig. 11A). The earliest palaeosol (Palaeosol A: Unit E) overlies Unit D and represents a fairly widespread development of soil. It extends both east and west of BBC and was probably continuous in front of the cave. Just west of BBC, the weakly developed Palaeosol B (Unit G) is separated from Palaeosol A by a thin, massive sand unit, whereas the two soils are separated by a thick unit of dune cross-bedding 0.5–1 km farther west. A similar sequence of cross-bedded sand separates Palaeosol B from Palaeosol C (Unit I) to the west of BBC, but there is little separation in the multi-soil area. Palaeosol C, which is slightly redder than the two underlying soils, may represent a longer period of non-deposition in the Blombos area. The elevations of all three palaeosols range from 28 to 34 m amsl, similar to the height of the cave opening (~34.5 m amsl). These soils may have extended at similar elevations in front, and to the east, of BBC, providing easy access to the cave during periods of landscape stability. The upper layers of phase M3 inside BBC contain the highest density of shell, fauna and stone artefacts, which suggests that ease of access to the site may have facilitated frequent and intense occupation.

These successions of dune cross-beds and soil profiles indicate either variably drier and wetter rainfall patterns or variations in wind strength, with the dominant wind direction towards the east. For phase M3 (layers CN/CO, CL, CK and CJ), an increase in humidity is supported by $\delta^{18}O$ values for ostrich eggshell, and winter rainfall conditions are indicated by the $\delta^{13}C$ values for the same samples (Roberts et al., 2016). These interpretations are consistent with greater rainfall promoting palaeosol formation. A change appears in layer CI/CH, with more enriched isotopic ratios suggesting a shift towards drier conditions and rainfall throughout the year.

Rhizomorphs and remains of land snails in all three palaeosols indicate a moderate vegetation cover during this period (96–82 ka). Soils likely also formed on the exposed inshore outcrops of Mesozoic Kirkwood Formation (Fig. 11A), as they had significant time to form soils since the regression of sea-level from a position close to the current coast during MIS 5e. These rocks promote deep and moderately fertile loamy soils (Cawthra et al., this issue), that Cowling et al. (this issue) suggest carried Renosterveld vegetation. This is consistent with the $\delta^{13}C$ values for ostrich eggshell that suggest the presence of $C_3$ vegetation (shrubs and trees) up to and including layer CJ, with those for layer CI/CH suggesting a transition to more aridity-linked CAM vegetation (e.g., succulents). The faunal assemblage from layers CJ and CI/CH is dominated by *Raphicerus* sp. (steenbok/grysbok), *Procavia capensis* (rock hyrax), *Bathyergus suillus* (Cape dune molerat) and *Arctocephalus pusillus* (Cape fur seal). These animals suggest the presence of aeolianite cliffs, sandy substrate, proximity to the ocean, and shrubland vegetation (Henshilwood et al., 2001a; Badenhorst et al., 2016). The other layers in phase M3 have small numbers of specimens, limiting the environmental inferences that can be drawn.

The malacological assemblage is also dominated by remains from layers CJ and CI/CH, where shells form clast-supported layers (Fig. 2B) and constitute the highest density of shellfish remains in the cave. These two layers have shellfish densities of 123 and 103 kg/m$^3$, respectively, which is around 4–28 times greater than those of any other layers in phase M3 (Roberts et al., 2016). *Turbo sarmaticus*, *Patella* sp. and *Dinoplax gigas* dominate the assemblage; all are rocky intertidal species that would have been available on the enlarged expanse of rocky coast throughout much of this period (Fig. 11A). *Perna perna*, which occupies the same environmental niche, is present in lower abundance. Roberts et al. (2016) also interpreted the proportional contributions of the warm-water adapted *Cymbula oculus* and cold-water adapted *C. granatina* as possible evidence of an increased incidence of near-shore upwelling, easterly winds, summer rainfall and increased $C_4$ vegetation (grasses) in the region. An increased presence of *C. granatina* appears towards the end of phase M3 in layers CJ and

CI/CH, but the apparent spike in the middle of phase M3 (layers CN/CO and CM) is likely not statistically significant, given the very small size of the assemblage.

The cross-bedded aeolian deposits of Units D, F and I show mostly eastward dipping cross-beds, produced by predominantly westerly winds, and in layer CJ the $\delta^{18}O$ and $\delta^{13}C$ isotopic ratios for ostrich eggshell suggest higher humidity, winter rainfall and $C_3$ vegetation. This is consistent with the findings of Roberts et al. (2013), who suggest that prevailing westerly- and southwesterly winds dominated throughout the Pleistocene. Environmental conditions had changed by the time of deposition of layer CH, which marks the end of phase M3 and is younger than the other M3 deposits (Table 1). It is difficult to distinguish between layers CI and CH in places, however, because of the density of shell. The two layers are, therefore, commonly combined for analysis, but this may be problematic for resolving when this change occurred and how it may have affected human occupation and subsistence at BBC.

As with the faunal assemblages, artefact density in phase M3 is highest in the upper layers (CIBh2, CIB, CIA and CI/CH), where silcrete is the dominant raw material for stone artefact production (Douze et al., 2015). The main characteristic of the assemblage is the predetermination of blank shapes by core reduction; retouched tools are very rare. Douze et al. (2015) suggested that this assemblage can be grouped as a single MSA tradition. The upper layers (CJ and CI/CH) of phase M3 also include 10 pieces of deliberately engraved ochre (Henshilwood et al., 2009).

### *5.3 Occupation during phase M2 lower*

The top of phase M3 (layer CH) and all of phase M2 lower represent a continuation from the underlying layers and the corresponding landscape units, and correlate chronologically with Unit J (Fig. 12), which was deposited between the peak of MIS 5b (87 ka) and the end of MIS 5a (76 ka). This time interval includes a sea-level transgression to –20 m bmsl and the subsequent regression to –40 m bmsl at ~76 ka. Sediment deposition outside the cave initially followed a similar pattern to that of the preceding period, with a thin palaeosol sandwiched between two dune sands. Near the top of this sequence, the dune grades into a soil in some places and into sheetwash deposits elsewhere (Fig. 5). Common rhizomorphs provide evidence that the dunes were vegetated, but without large-scale pedogenesis. This suggests a reduction in rainfall, which is supported by the aridity trend observed in the isotopic ratios from ostrich eggshell. The fauna and shellfish assemblages for this period show similar patterns to those recorded for phase M3. Small browsers continue to dominate (Thompson and Henshilwood, 2011), suggesting a persisting shrubland environment, and the proportion of cold-water adapted *C. granatina* remains high (Roberts et al., 2016), perhaps signifying the presence of upwelling along the coast. Overall, the densities of all assemblages are low. Archaeologically, the layers comprising phase M2 lower are characterised by a series of basin-shaped hearths, small quantities of blades, flakes and cores (made from silcrete, quartz and quartzite), and some small ochre pieces. Some of the latter have been ground or scraped, but none bear deliberate engravings (Henshilwood et al., 2001a; Henshilwood and van Niekerk, 2014).

Up to this time of occupation at BBC (~76 ka), sea level has not fallen lower than about –50 m bmsl, which places the coastline only ~3.5 km from its present position (Fig. 11A). The coastal plain remained predominantly rocky, with sand availability indicated by the formation of a coastal calcareous dune cordon by mainly westerly winds blowing along the shore. These pulses of massive sand input (Figs 5, 7 and 12) were presumably mobilised during sea-level oscillations. This situation is very similar to the modern setting, except that BBC was located farther away from the coast than it is today.

*5.4 Occupation during phases M2 upper and M1*

None of the onshore sediments currently preserved are coeval with sediments associated with the M2 upper and M1 phases (the Still Bay archaeological layers), which are dated to between 76 ± 3 and 71 ± 4 ka (Fig. 12). This time gap is represented outside BBC by an erosional boundary that separates Units J and below from Unit K, the top dune in the stratigraphic sequence. These younger dunes overlie Units J or I in some places, but elsewhere extend down to cover Unit E and older units, including the Table Mountain Group. To interpret these phases, therefore, we have to look to the offshore record.

The M2 upper and M1 phases contain the first evidence of Still Bay-type bifacial foliate points, which were used as projectiles and multi-purpose tools (Lombard, 2007). Some of the points made from silcrete were heat-treated and finely shaped using pressure flaking (Villa et al., 2009). The Still Bay points are associated with bone points and awls (Henshilwood et al., 2001b, 2002; d'Errico et al., 2007), engraved bone (d'Errico et al., 2001), multiple pieces of ochre, including eight deliberately engraved with cross-hatched patterns (Henshilwood et al., 2001a, 2002, 2009), more than fifty *Nassarius kraussianus* shell beads (Henshilwood et al., 2004; d'Errico et al., 2005; Vanhaeren et al., 2013) and a cross-hatched drawing made with an ochre crayon on a silcrete flake (Henshilwood et al., 2018).

During deposition of phase M2 upper (layers CFD to CFA) between 76 ± 3 and 74 ± 2 ka, sea levels remained at similar elevations to the preceding archaeological phases (M3 lower and M3), so the coast was never further away than ~3.5 km from BBC. The faunal assemblage was similarly dominated by rock hyrax and steenbok/grysbok, suggesting shrubland environments (Reynard and Henshilwood, 2018a,b). Scrubland and bush vegetation around the cave is also reflected in the microfauna (Nel and Henshilwood, 2016). Rocky intertidal shellfish species are most prevalent during this period. Oxygen isotopic ratios from ostrich eggshell exhibit a continuing trend (relative to the underlying layers) of increasing aridity, and the carbon isotopic ratios are similar to those obtained for eggshell from near the top of phase M3, suggesting a shift towards year-round rainfall and aridity-linked CAM vegetation (Roberts et al., 2016).

Phase M1 is associated with a period of accelerated fall in sea level to below –50 m bmsl, resulting, for the first time in the occupation of BBC, in a greatly expanded coastal plain from ~73 ka (Fig. 11B). The local rivers had broad floodplains terminating in estuaries. Cowling et al. (this issue) suggest that the floodplain deposits were associated with alluvial savannah vegetation, and that the intervening Buffelskloof and Kirkwood Formations (Fig. 11B), carried grassland to the east of BBC and Renosterveld to the west. Throughout phase M1 (layers CD–CA), there is an overall reduction in the number of browsers and an increase in the number of large ungulate grazers, such as eland, buffalo and wildesbeest/hartebeest, reflecting the expansion of the coastal plain (Thompson and Henshilwood, 2011; Discamps and Henshilwood, 2015). Also present in these assemblages are the remains of hippopotamus, which rely on the availability of rivers and lakes, as well as grassland for grazing. The eastward-flowing Breede and Duiwenhoks Rivers would have supported these animals and provided a reliable source of freshwater for hunter-gatherer communities (Fig. 11B). Collection of algae and sea-grasses from the rivers and estuaries may also provide support for the presence of *Nassarius kraussianus* shells in these deposits. Fossil trackways of elephant, giraffe, giant Cape horse, hippopotamus, rhinoceros and buffalo have been described from along the coast of Still Bay (e.g., Helm et al., this issue). The microfauna also show a shift to more open and moist grasslands, with the micromammal composition of layers CCC–CA reflecting very rapid environmental change; the habitat changes were so significant that some micromammal species disappeared (Nel and Henshilwood, 2016). The shellfish remains are similar in composition to

that of phase M2, dominated by warm-water rocky intertidal species. *Donax serra* (sand mussel) appears for the first time, albeit in relatively low abundance. This species requires access to sandy beaches that were never very close to BBC; we estimate that the closest sandy beaches were ~3.5 km away during the M1 phase. Although the coastline was never more than ~10.5 km away from the cave at this time, the expanded coastal plain significantly changed the quantity and variety of resources available to the inhabitants of BBC, as is reflected in their changing subsistence patterns.

### *5.5 Closure and abandonment of BBC*

At the end of MIS 5a and the start of MIS 4 (~71 ka), a period of coastal sand dune accumulation began again as sea levels fell to at least –72 m bmsl (Fig. 11C). At this time, the coastline lay at least 16–30 km from BBC. Sand was probably blown up to the top of the escarpment from the indented bay farther west, to form a broad sand cap overlying the Table Mountain Group and Wankoe Formation. Remnants of this sand cover are still present today at elevations of 100–130 m amsl. A shift in climate allowed more northerly winds to become dominant, mobilising sand at the top of the escarpment. Large quantities of sand were blown over the edge of the cliff, accumulating as large angle-of-repose dunes with southward-dipping foreset beds, draped across the partially eroded remains of the earlier MIS 5 succession. This cross-bedding is best seen in modern gullies cut into these deposits near the base of the upper cliffs.

The top dune (Unit K) directly overlies Palaeosol C in places, while in others it extends down to cover Palaeosol A and all older units, including the Table Mountain Group. Jacobs et al (2003a) reported two single-aliquot OSL ages for the youngest dune sequence at BBC: 69.6 ± 3.5 ka (ZB13) for a sand dune outside, but at the same altitude as, the cave; and 70.9 ± 2.8 ka (ZB20) for a cemented coastal stack overlying the Table Mountain Group and in line with the cave entrance. Sample ZB15, collected from the stratigraphically equivalent layer of sterile sand overlying the most recent MSA occupation, yielded single-aliquot and single-grain ages of 69.2 ± 3.9 and 67.3 ± 3.8 ka, respectively (Jacobs et al., 2003a,b). Unit K appears to have formed a near-continuous sand cover along the Blombos coast and would likely have buried the entrance to BBC, terminating occupation and preserving the cave contents.

At some stage after this last phase of dune deposition, calcrete started to form along parts of the coast. It is well preserved 1.2–1.3 km west of BBC, where it partially covers both Unit K (MIS 4) and Unit B (MIS 11). Calcrete may still be forming at the present time and is responsible for the more prominent cementation in this part of the study area. It has probably formed as a result of groundwater discharge from the lower section of the Waenhuiskrans Formation, possibly where it intersects the underlying Wankoe Formation or Table Mountain Group.

The Pleistocene dune deposits in front of BBC were not removed until after the post-glacial transgression, perhaps when Holocene sea levels reached 1–2 m amsl. The re-opening of BBC allowed Later Stone Age occupation from ~2 ka until ~290 yr BP (Thompson and Henshilwood, 2011), separated from the MSA levels by the layer of dune sand deposited ~70 ka.

## 6. Conclusions

In this study, we have used the timing and nature of landscape-scale depositional processes to inform on site formation and MSA occupation of BBC during MIS 5 and the transition to MIS 4. This approach offers the opportunity to understand changing modes of sediment deposition, their relationship to fluctuating sea levels, and the concomitant exposure and/or inundation of the Agulhas Bank. Together, these large-scale changes, expressed as palaeosols during periods

of landscape stability and as dune deposition during periods of instability associated with rapid oscillations in sea level, provide the backdrop against which we can track the presence or absence of humans at BBC. The presence of palaeosols and dunes on the landscape also has the potential to inform on rates of sediment deposition inside BBC and, hence, occupation intensity; sediment input appears to have been irregular.

Combining the timescale developed for BBC with that for its surrounding environment has allowed us to integrate the broader onshore and offshore landscape record with the different environmental proxies extracted from finds associated with the three main phases of cave occupation. For most of this period, the environmental conditions were similar to those at the present day. The coastline remained rocky, supporting a rich shellfish community for subsistence. Winter rainfall conditions promoted soil formation that supported predominantly $C_3$ vegetation and small-sized browsers. Only towards the end of occupation, during the final stages of phase M1, did further significant changes occur, as the now-submerged palaeo-Agulhas Plain started to expand further and major rivers flowed eastwards and closer to BBC. This introduced new types of savannah grassland vegetation along the floodplains, practically on the doorstep of BBC, bringing with it new types of food resources for human consumption. This shift to $C_4$ vegetation and large grazing bovids is reflected in the assemblages of the final MSA (Still Bay) layers in BBC.

This changing climate and dynamic environment was responsible for the closure and preservation of BBC. Large coastal dunes blew in from the exposed shelf and over the top of the escarpment, filling and covering BBC until the late Holocene, when the dune blanket was undercut and eroded by higher sea levels. In the period between closure of the cave and its reopening, people were likely still present on this fertile landscape and sought shelter elsewhere, unaware of the cave that had been home to many earlier generations.

We consider that this coarse-scale study of landscape-scale processes is essential to provide a more complete understanding of the broader context of human occupation of the south Cape coast, as well as other regions, forming the basis for better-informed integration of finer-scale interpretations of the archaeological, sedimentary and environmental patterns detected in the BBC records.

## Acknowledgements

This research was funded by the Australian Research Council through Discovery Project grants DP0666084 (Roberts and Jacobs) and DP1092843 (Jacobs). We thank Elspeth Hayes for assistance in the field and Terry Lachlan, Yasaman Jafari and Lauren Linnenlucke for laboratory assistance.

## References

Aitken, M.J., 1998. An Introduction to Optical Dating. Oxford University Press, Oxford.

Badenhorst, S., Van Niekerk, K.L., Henshilwood, C.S., 2016. Large mammal remains from 100 ka Middle Stone Age layers of Blombos Cave, South Africa. South African Archaeological Bulletin 71, 46–52.

Bateman, M.D., Holmes, P.J., Carr, A.S., Horton B.P., Jaiswal, M.K., 2004. Aeolianite and barrier dune construction spanning the last two glacial-interglacial cycles from the southern Cape Coast, South Africa. Quaternary Science Reviews 23, 1681–1698.

Bronk Ramsey, C., 2009a. Bayesian analysis of radiocarbon dates. Radiocarbon 51, 337–360.

Bronk Ramsey, C., 2009b. Dealing with outliers and offsets in radiocarbon dating. Radiocarbon 51, 1023–1045.

Bronk Ramsey, C., Lee, S., 2013. Recent and planned developments of the program OxCal. Radiocarbon 55, 720–730.

Carr, A.S., Bateman, M.D., Roberts, D.L., Murray-Wallace, C.V., Jacobs, Z., Holmes, P.J., 2010. The last interglacial sea-level high stand on the southern Cape coastline of South Africa. Quaternary Research 73, 351–363.

Cawthra, H.C., Cowling, R.M., Ando, S., Marean, C.W., this issue. Geological and soil maps of the palaeo-Agulhas Plain for the Last Glacial Maximum. Quaternary Science Reviews (Special Publication on the palaeo-Agulhas Plain).

Cawthra, H.C., Compton, J.S., Fisher, E.C., MacHutchon, M.R., Marean, C.W., 2016. Submerged shorelines and landscape features offshore of Mossel Bay, South Africa. In: Harff, J., Bailey, G., Lüth, F. (Eds) Geology and Archaeology: submerged landscapes of the continental shelf. Geological Society of London, Special Publication 411, 219–233.

Cawthra, H.C., Jacobs, Z., Compton, J.S., Fisher, E.C., Karkanas, P., Marean, C.W., 2018. Depositional and sea-level history from MIS 6 (Termination II) to MIS 3 on the southern shelf of South Africa. Quaternary Science Reviews 181, 156–172.

Compton, J.S., 2011. Pleistocene sea-level fluctuations and human evolution on the southern coastal plain of South Africa. Quaternary Science Reviews 30, 506–527.

Cowling, R.M., Potts, A.J., Franklin, J., Marean, C.W., this issue. Describing a drowned ecosystem: Last Glacial Maximum vegetation reconstruction of the palaeo-Agulhas Plain. Quaternary Science Reviews (Special Publication on the palaeo-Agulhas Plain).

d'Errico, F., Henshilwood, C.S., Nilssen, P., 2001. An engraved bone fragment from ca. 70 ka year old Middle Stone Age levels at Blombos Cave, South Africa: implications for the origin of symbolism and language. Antiquity 73, 309–318.

d'Errico, F., Henshilwood, C., Vanhaeren, M., Van Niekerk, K., 2005. *Nassarius kraussianus* shell beads from Blombos Cave: evidence for symbolic behaviour in the Middle Stone Age. Journal of Human Evolution 48, 3–24.

d'Errico, F., Henshilwood, C.S., 2007. Additional evidence for bone technology in the southern African Middle Stone Age. Journal of Human Evolution 52, 142–163.

Discamps, E., Henshilwood, C.S., 2015. Intra-site variability in the Still Bay fauna at Blombos Cave: implications for explanatory models of the Middle Stone Age cultural and technological evolution. PLoS One 10, e0144866.

Douze, K., Wurz, S., Henshilwood, C.S., 2015. Techno-cultural characterization of the MIS 5 (c. 105–90 ka) lithic industries at Blombos Cave, southern Cape, South Africa. PLoS One 10, e0142151.

Duller, G.A.T., 2004. Luminescence dating of Quaternary sediments: recent advances. Journal of Quaternary Science 19, 183–192.

Ekau, W. and cruise participants, 2014. Training and Capacity Building Cruise. R.V. Meteor cruise M102, 6–23 December 2013, Le Port (Réunion) to Walvis Bay (Namibia). DFG-Senatskommission für Ozeanographie, Bremen.

Fisher, E.C., Bar-Matthews, M., Jerardino, A., Marean, C., 2010. Middle and Late Pleistocene paleoscape modeling along the southern coast of South Africa. Quaternary Science Reviews 29, 1382–1398.

Galbraith, R.F., Roberts, R.G., Laslett, G.M., Yoshida, H., Olley, J.M., 1999. Optical dating of single and multiple grains of quartz from Jinmium rock shelter, northern Australia, Part I: experimental design and statistical models. Archaeometry 41, 339–364.

Hahn, A., Schefu□, E., Andò, S., Cawthra, H.C., Frenzel, P., Kugel, M., Meschner, S., Mollenhauer, G., Zabel, M., 2017. Southern Hemisphere anticyclonic circulation drives oceanic and climatic conditions in late Holocene southernmost Africa. Climate of the Past 13, 649–665.

Helm, C.W., Cawthra, H.C., Cowling, R.M., de Vynck, J., Lockley, M.G., Marean, C.W., Thesen, G.H.H., Venter, J., this issue. Pleistocene vertebrate tracksites on the south Cape coast of South Africa and their potential palaeoecological implications. Quaternary Science Reviews (Special Publication on the palaeo-Agulhas Plain).

Helm, C.W., Cawthra, H.C., Cowling, R.M., De Vynck, J.C., Marean, C.W., McCrea, R.T., Rust, R. 2018. Palaeoecology of giraffe tracks in Late Pleistocene aeolianites on the Cape south coast. South African Journal of Science 114, 67–74.

Henshilwood, C. S., Dubreuil, B., 2011. The Still Bay and Howiesons Poort, 77–59 ka: Perspective-taking and the evolution of the modern human mind during the African Middle Stone Age. Current Anthropology 52, 361–400.

Henshilwood, C.S., van Niekerk, K.L., 2014. Blombos Cave: the Middle Stone Age levels. In: Smith, C. (Ed.) Encyclopedia of Global Archaeology, 915–922. Springer, New York.

Henshilwood, C.S., Sealy, J.C., Yates, R., Cruz-Uribe, K., Goldberg, P., Grine, F.E., Klein, R.G.,Poggenpoel, C., Van Niekerk, K., Watts, I., 2001a. Blombos Cave, southern Cape, South Africa: preliminary report on the 1992–1999 excavations of the Middle Stone Age levels. Journal of Archaeological Science 28, 421–448.

Henshilwood, C.S., d'Errico, F., Marean, C.W., Milo, R.G., Yates, R.J., 2001b. An early bone tool industry from the Middle Stone Age, Blombos Cave, South Africa: implications for the origins of modern human behaviour, symbolism and language. Journal of Human Evolution 41, 631–678.

Henshilwood, C.S., d'Errico, F., Yates, R., Jacobs, Z., Tribolo, C., Duller, G.A.T., Mercier, N., Sealy, J.C., Valladas, H., Watts, I., Wintle, A.G., 2002. Emergence of modern human behaviour: Middle Stone Age engravings from South Africa. Science 295, 1278–1280.

Henshilwood, C., d'Errico, F., Vanhaeren, M., van Niekerk, K., Jacobs, Z., 2004. Middle Stone Age shell beads from South Africa. Science 304, 404.

Henshilwood, C.S., d'Errico, F., Watts, I., 2009. Engraved ochres from the Middle Stone Age levels at Blombos Cave, South Africa. Journal of Human Evolution 57, 27–47.

Henshilwood, C.S., d'Errico, F., van Niekerk, K.L., Coquinot, Y., Jacobs, Z., Lauritzen, S.-E., Menu, M., García-Moreno, R., 2011. A 100,000-year-old ochre-processing workshop at Blombos Cave, South Africa. Science 334, 219–222.

Henshilwood, C.S., van Niekerk, K.L., Wurz, S., Delagnes, A., Armitage, S.J., Rifken, R.F., Douze, K., Keene, P., Haaland, M.M., Reynard, J., Discamps, E., Mienies, S.S., 2014. Klipdrift Shelter, southern Cape, South Africa: preliminary report on the Howiesons Poort layers. Journal of Archaeological Science 45, 284–303.

Henshilwood, C.S., d'Errico, F., van Niekerk, K.L., Dayet, l., Queffelec, A., Pollarolo, L. 2018. An abstract drawing from the 73,000 year old levels at Blombos Cave, South Africa. Nature 562, 115–118.

Hillestad-Nel, T., Henshilwood, C.S., 2016. The small mammal sequence from the c. 76–72 ka Still Bay levels at Blombos Cave, South Africa – taphonomic and palaeoecological implications for human behaviour. PLoS One 11, e0159817.

Hu, Y., Marwick, B., Zhang, J.-F., Rui, X., Hou, Y.-M., Yue, J.-P., Chen, W.-R., Huang, W.-W., Li, B., 2019. Late Middle Pleistocene Levallois stone-tool technology in southwest China. Nature 565, 82–85.

Huntley, D.J., Godfrey-Smith, D.I., Thewalt, M.L.W., 1985. Optical dating of sediments. Nature 313, 105–107.

Jacobs, Z., Roberts, R.G., 2015. An improved single grain OSL chronology for the sedimentary deposits from Diepkloof Rockshelter, Western Cape, South Africa. Journal of Archaeological Science 63, 175–192.

Jacobs, Z., Roberts, R.G., 2017. Single-grain OSL chronologies for the Still Bay and Howieson's Poort industries and the transition between them: further analyses and statistical modelling. Journal of Human Evolution 107, 1–13.

Jacobs, Z., Wintle, A.G., Duller, G.A.T., 2003a. Optical dating of dune sand from Blombos Cave, South Africa: I—multiple grain data. Journal of Human Evolution 44, 599–612.

Jacobs, Z., Duller, G.A.T., Wintle, A.G., 2003b. Optical dating of dune sand from Blombos Cave, South Africa: II—single grain data. Journal of Human Evolution 44, 613–625.

Jacobs, Z., Duller, G.A.T., Wintle, A.G., Henshilwood, C.S., 2006. Extending the chronology of deposits at Blombos Cave, South Africa, back to 140 ka using optical dating of single and multiple grains of quartz. Journal of Human Evolution 51, 255–273.

Jacobs, Z., Roberts, R.G., Lachlan, T.J., Karkanas, P., Marean, C.W., Roberts, D.L., 2011. Development of the SAR TT-OSL procedure for dating Middle Pleistocene dune and shallow marine deposits along the southern Cape coast of South Africa. Quaternary Geochronology 6, 491–513.

Jacobs, Z., Hayes, E.H., Roberts, R.G., Galbraith, R.F., Henshilwood, C.S., 2013. An improved OSL chronology for the Still Bay layers at Blombos Cave, South Africa: further tests of single-grain dating procedures and a re-evaluation of the timing of the Still Bay industry across southern Africa. Journal of Archaeological Science 40, 579–594.

Jones, H.L., 2001. Electron spin resonance dating of tooth enamel at three Palaeolithic sites. Ph.D. dissertation, McMaster University.

Karkanas, P., Brown, K.S., Fisher, E.C., Jacobs, Z., Marean, C.W., 2015. Interpreting human behaviour from depositional rates and combustion features through the study of sedimentary microfacies at site Pinnacle Point 5-6, South Africa. Journal of Human Evolution 85, 1–21.

Langejans, G.H.J., Dusseldorp, G.L., Henshilwood, C.S., 2012. Terrestrial gastropods from Blombos Cave, South Africa: research potential. South African Archaeological Bulletin 67, 120–144.

Li, B., Jacobs, Z., Roberts, R.G., 2016. Investigation of the applicability of standardised growth curves for OSL dating of quartz from Haua Fteah cave, Libya. Quaternary Geochronology 35, 1–15.

Li, B., Jacobs, Z., Roberts, R.G., Galbraith, R., Peng, J., 2017. Variability in quartz OSL signals caused by measurement uncertainties: problems and solutions. Quaternary Geochronology 41, 11–25.

Lisiecki, L.E., Raymo, M.E. 2005. A Pliocene-Pleistocene stack of 57 globally distributed benthic $\delta^{18}O$ records. Paleoceanography 20, PA1003.

Lombard, M., 2007. Evidence for change in Middle Stone Age hunting behaviour at Blombos Cave: results of a macrofracture analysis**.** South African Archaeological Bulletin 62, 62–67.

Marean, C.W., 2010. Pinnacle Point 13B (western Cape, South Africa) in context: the Cape Floral Kingdom, shellfish and modern human origins. Journal of Human Evolution 59, 425–443.

Marean, C.W., Goldberg, P., Avery, G., Grine, F.E., Klein, R.G., 2000. Last Interglacial Stone Age stratigraphy and excavations at Die Kelders Cave 1 (Western Cape Province, South Africa): the 1992, 1993 and 1995 field seasons. Journal of Human Evolution 38, 7–42.

Mourre, V., Villa, P., Henshilwood, C.S., 2010. Early use of pressure flaking on lithic artifacts at Blombos Cave, South Africa. Science 330, 659–662.

Reynard, J.P., Badenhorst, S., Henshilwood C.S., 2014. Inferring animal size from the unidentified long bones from the Middle Stone Age layers at Blombos Cave, South Africa. Annals of the Ditsong National Museum of Natural History (Annals of the Transvaal Museum) 4, 9–25.

Reynard, J., Henshilwood, C.S., 2017. Subsistence strategies during the later Middle Stone Age in the southern Cape of South Africa: comparing the Still Bay of Blombos Cave with the Howiesons Poort of Klipdrift Shelter. Journal of Human Evolution 108, 110–130.

Reynard, J.P., Henshilwood, C.S., 2018a. Using trampling modification to infer occupational intensity during the Still Bay at Blombos Cave, southern Cape, South Africa. African Archaeological Review 35, 1–19.

Reynard, J., Henshilwood, C.S., 2018b. Environment versus behaviour: zooarchaeological and taphonomic analyses of fauna from the Still Bay layers at Blombos Cave, South Africa. Quaternary International.

Rhodes, E.J., Bronk Ramsey, C., Outram, Z., Batt, C., Willis, L., Dockrill, S., Bond, J., 2003. Bayesian methods applied to the interpretation of multiple OSL dates: high precision sediment ages from Old Scatness Broch excavations, Shetland Isles. Quaternary Science Reviews 22, 1231–1244.

Roberts, D.L., Bateman, M.D., Murray-Wallace, C.V., Carr, A.S., Holmes, P.J., 2008. Last Interglacial fossil elephant trackways dated by OSL/AAR in coastal aeolianites, Still Bay, South Africa. Palaeogeography, Palaeoclimatology, Palaeoecology 257, 261–279.

Roberts, D.L., Karkanas, P., Jacobs, Z., Marean, C.W., Roberts, R.G., 2012. Melting ice sheets 400,000 yr ago raised sea level by 13 m: past analogue for future trends. Earth and Planetary Science Letters 357–358, 226–237.

Roberts, D.L., Cawthra, H.C., Musekiwa, C., 2013. Dynamics of late Cenozoic aeolian deposition along the South African coast: a record of evolving climate and ecosystems. In: Martini, I.P., Wanless, H.R. (Eds) Sedimentary Coastal Zones from High to Low Latitudes: similarities and differences. Geological Society of London, Special Publication 388, 353–387.

Roberts, R.G., Jacobs, Z., Li, B., Jankowski, N.R., Cunningham, A.C., Rosenfeld, A.B., 2015. Optical dating in archaeology: thirty years in retrospect and grand challenges for the future. Journal of Archaeological Science 56, 41–60.

Roberts, P., Henshilwood, C.S., van Niekerk, K.L., Keene, P., Gledhill, A., Reynard, J., Badenhorst, S., Lee-Thorp, J., 2016. Climate, environment and early human innovation: stable isotope and faunal proxy evidence from archaeological sites (98–59 ka) in the southern Cape, South Africa. PLoS One 11, e0157408.

Smith, E.I., Jacobs, Z., Johnsen, R., Ren, M., Fisher, E.C., Oestmo, S., Wilkins, J., Harris, J.A., Karkanas, P., Fitch, S., Ciravolo, A., Keenan, D., Cleghorn, N., Lane, C.S., Matthews, T., Marean, C.W., 2018. Humans thrived in South Africa through the Toba eruption about 74,000 years ago. Nature 555, 511–515.

Thompson, J.C., Henshilwood, C.S., 2011. Taphonomic analysis of the Middle Stone Age larger mammal faunal assemblage from Blombos Cave, southern Cape, South Africa. Journal of Human Evolution 60, 746–767.

Thompson, J., Henshilwood, C.S., 2014. Nutritional values of Middle Stone Age tortoises at Blombos Cave, South Africa, and implications for foraging and social behaviour. Journal of Human Evolution 67, 33–47.

Thompson, J., Henshilwood, C.S., 2014. Tortoise taphonomy and tortoise butchery patterns at Blombos Cave, South Africa. Journal of Archaeological Science 41, 214–229.

Tribolo, C., Mercier, N., Selo, M., Valladas, H., Joron, J.-L., Reyss, J.-L., Henshilwood, C.S., Sealy, J., Yates, R., 2006. TL dating of burnt lithics from Blombos Cave (South Africa): further evidence for the antiquity of modern human behaviour. Archaeometry 48, 341–357.

Vanhaeren, M., d'Errico, F., van Niekerk, K.L., Henshilwood, C.S., Erasmus, R.M., 2013. Thinking strings: additional evidence for personal ornament use in the Middle Stone Age at Blombos Cave, South Africa. Journal of Human Evolution 64, 500–517.

Villa, P., Soressi, M., Henshilwood, C.S., Mourre, V., 2009. The Still Bay points of Blombos Cave (South Africa). Journal of Archaeological Science 36, 441–460.

Waelbroeck, C., Labeyrie, L., Michel, E., Duplessy, J.C., McManus, J.F., Lambeck, K., Balbon, E., Labracherie, M., 2002. Sea-level and deep water temperature changes derived from benthic foraminifera isotopic records. Quaternary Science Reviews 21, 295–305.

Wintle, A.G., 2014. Luminescence dating methods. In: Holland, H., Turekian, K. (Eds) Treatise on Geochemistry (2nd edition) 14, 17–35. Elsevier, Oxford.

Zabel, M. and cruise participants, 2017. Climate Archives in Coastal Waters of Southern Africa. R.V. Meteor cruise M123, 3–27 February 2016, Walvis Bay (Namibia) to Cape Town (South Africa). DFG-Senatskommission für Ozeanographie, Bremen.

**Figure captions**

**Figure 1**: Locality map of the south Cape coast and the Middle Stone Age archaeological sites mentioned in the text. The –120 m isobath delimits the area exposed during the maximum sea level regression of the last glacial period (blue shading) and shows the broad shallow shelf extending off the south coast.

**Figure 2**: A, Planform map of Blombos Cave, showing the excavation grid (image courtesy of Magnus Haaland). B, Close-up photographs of squares G6c and G6d along the South Section wall, showing the individual layers and their relationships to the Middle Stone Age phases (right-hand column). C, Aerial view of the excavation area, with the black stippled lines demarcating the layer of cemented sand that underlies the lowest archaeological remains. D, Photograph of the entrance to the inner chamber at the back of the cave in square F2. E, Close-up photograph of some of the layers observed in the inner chamber, from which three samples were collected for OSL dating. F, Schematic drawing of the stratigraphic relationships between the layers and locations of OSL samples in the inner chamber.

**Figure 3**: Close-up image of the area immediately surrounding Blombos Cave (BBC), showing the position of the cave relative to the samples collected for OSL dating from four main areas outside the cave (numbered white diamonds) and to other surveyed features (TD, base of Unit K; LD, top of Table Mountain Group; WF, location of Unit C outcrop).

**Figure 4**: Bayesian model of OSL ages for deposits inside BBC. Ages (n = 37) have been modelled in OxCal version 4.2.4. Only random errors are included in the age model. Pale probability distributions represent the unmodelled ages (likelihoods) and dark grey distributions represent the modelled ages (posterior probabilities). The narrow and wide brackets beneath the distributions represent the 68.2% and 95.4% probability ranges, respectively. Start and end ages have been modelled for each *Phase* as transitional *Boundaries*, assuming no breaks in sedimentation, with age ranges (95.4% confidence interval, random-only errors) shown in thousands of years (ka) and rounded off to the closest century.

**Figure 5**: Measured sections at four different locations close to BBC (height above present mean sea level). Letters A–L correspond to the units described in the text, and locations of OSL samples (BBC10-G1 to -G11) are shown on the right-hand side.

**Figure 6**: A, Unit B lower marine sands west of BBC, showing the location of OSL sample BBC10-G6. B, Overlying top dune sands (Unit K) with OSL sample BBC10-G5 capped by flowstone calcrete (Unit L).

**Figure 7**: A, Large aeolian dune (Unit C) overlying a palaeosol capped by reworked calcareous nodules. B, Thinly laminated sands and footprint near the base of Unit C. C, Flat and cross-bedded lower dune unit (Unit D) near sea level below BBC, where it unconformably overlies the Table Mountain Group. D, Coarse shelly sand in the lower part of Unit D. E, Larger dune cross-bedded succession in the upper part of Unit D. F, Large tabular cross-bed sets showing variation in wind direction in Unit D. G and H, Very large dune extending down from the top of the escarpment (Unit K).

**Figure 8**: A, Palaeosol A (Unit E) forms a marker bed above the dune cross-bedded sand and is overlain by Palaeosols B (Unit G) and C (Unit J) in the multi-soil area. B, Location of OSL sample BBC10-G8 near the top of Unit E, where it is overlain by a dune (Unit F). C,

Structureless sand between Units E and G, with rhizomorphs in Unit G. OSL sample BBC10-G1 is from the lower part of Unit G.

**Figure 9**: A, Dune cross-bedding and location of OSL sample BBC10-G9 beneath Unit G. B, Onshore dipping cross-bed below Unit G at location of OSL sample BBC10-G7. C, Massive Unit J at location of OSL sample BBC10-G3. D, Location of OSL sample BBC10-G2, ~2 m below the top of Unit G. E, Sheetwash deposits in the lower part of the top dune sequence, directly overlying Unit J at location of OSL sample BBC10-G4. F, Abundant rhizomorphs in the upper part of Unit J that is partly covered by Unit K; the rhizomorphs extend down into the aeolian deposits at location of OSL sample BBC10-G4(2).

**Figure 10**: Three seismic profiles of transects on the Agulhas Bank near BBC: A, Perpendicular to the shoreline, west of BBC; B, Perpendicular to the shoreline, east of BBC; C, Parallel to the shoreline. Also shown are the interpretations of the seismic facies, together with sequence boundaries (solid lines) and evidence of incised channels (stippled lines). Seismic units shown are dunes/aeolianites; lagoon, floodplain and channel sediments; shelf sands; and bedrock which is both Palaeozoic and Mesozoic. The seismic profiles extend from water depths of 25 m at the shallowest to 80 m at the deepest.

**Figure 11**: Geological map for the region of the palaeo-Agulhas Plain (Cawthra et al., this issue) between the Breede and Gourits Rivers (west and east of BBC, respectively) and from the Cape Fold Belt mountains to the reconstructed shorelines at three sea levels: A, 50 m; B, 60 m; and C, 72 m below mean sea level.

**Figure 12**: Composite schematic drawings of the stratigraphic sequences found inside and outside BBC (left- and right-hand columns, respectively), together with the ages obtained for the various MSA phases and sedimentary units. The stippled lines between the two columns indicate the proposed correlations between the two sequences based on their respective chronologies.

**Table captions**

**Table 1**: Dose rate data, $D_e$ values and OSL ages for 40 sediment samples from inside Blombos Cave.

**Table 2**: OSL ages for Blombos Cave (shown as 'Unmodelled age ranges') and corresponding Bayesian age model estimates ('Modelled age ranges'), obtained using the OxCal 4.2.4 platform, at 68.2% and 95.4% probabilities. The modelled transition ages between each *Phase* are highlighted in bold and italics within the grey bands. All ages are given in years and rounded off to the closest decade.

**Table 3**: Grain size (μm) and mineralogy (%) of the Pleistocene dunes, soils (palaeosols) and calcrete cap.

**Table 4**: Dose rate data, $D_e$ values and OSL ages for 12 sediment samples from the measured sections outside Blombos Cave (see Fig. 5).

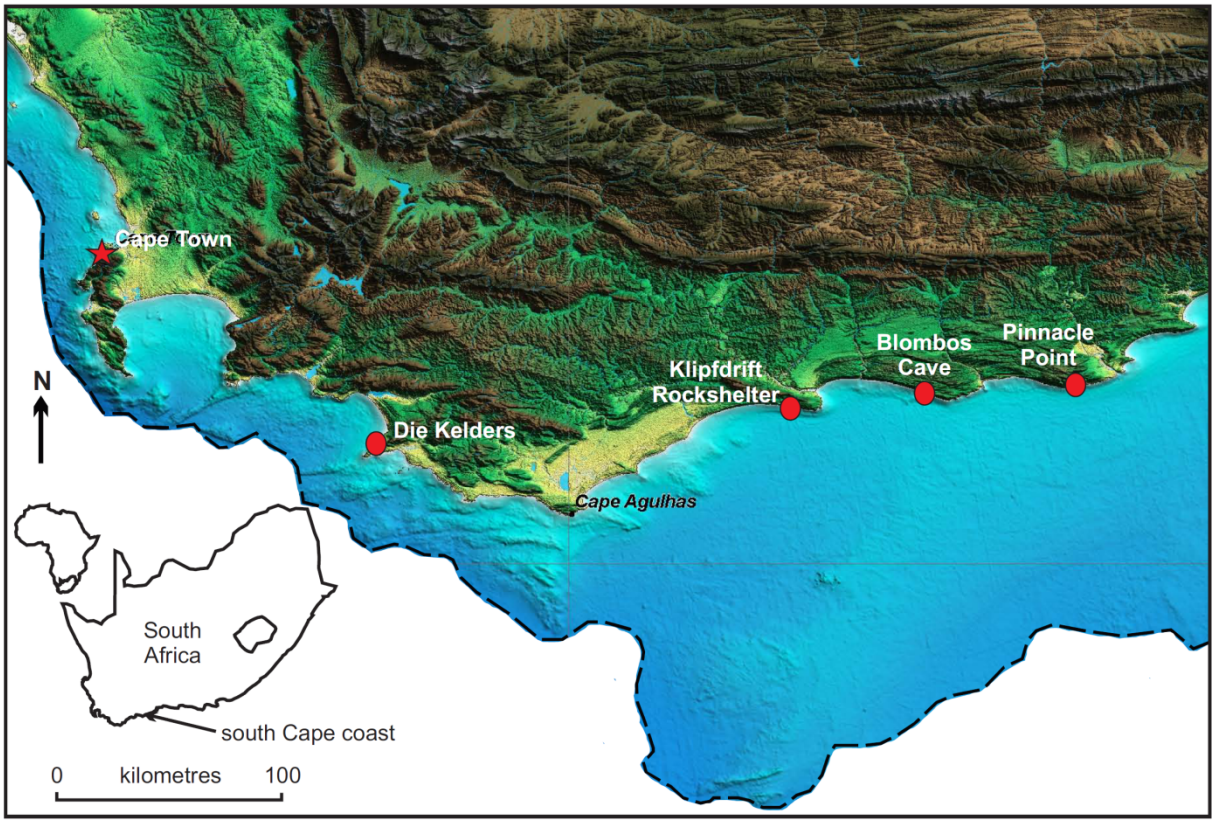
Cape Town
N
Die Kelders
Klipfdrift
Rockshelter
Blombos
Cave
Pinnacle
Point
Cape Agulhas
South
Africa
south Cape coast
0
kilometres
100

Figure 1:

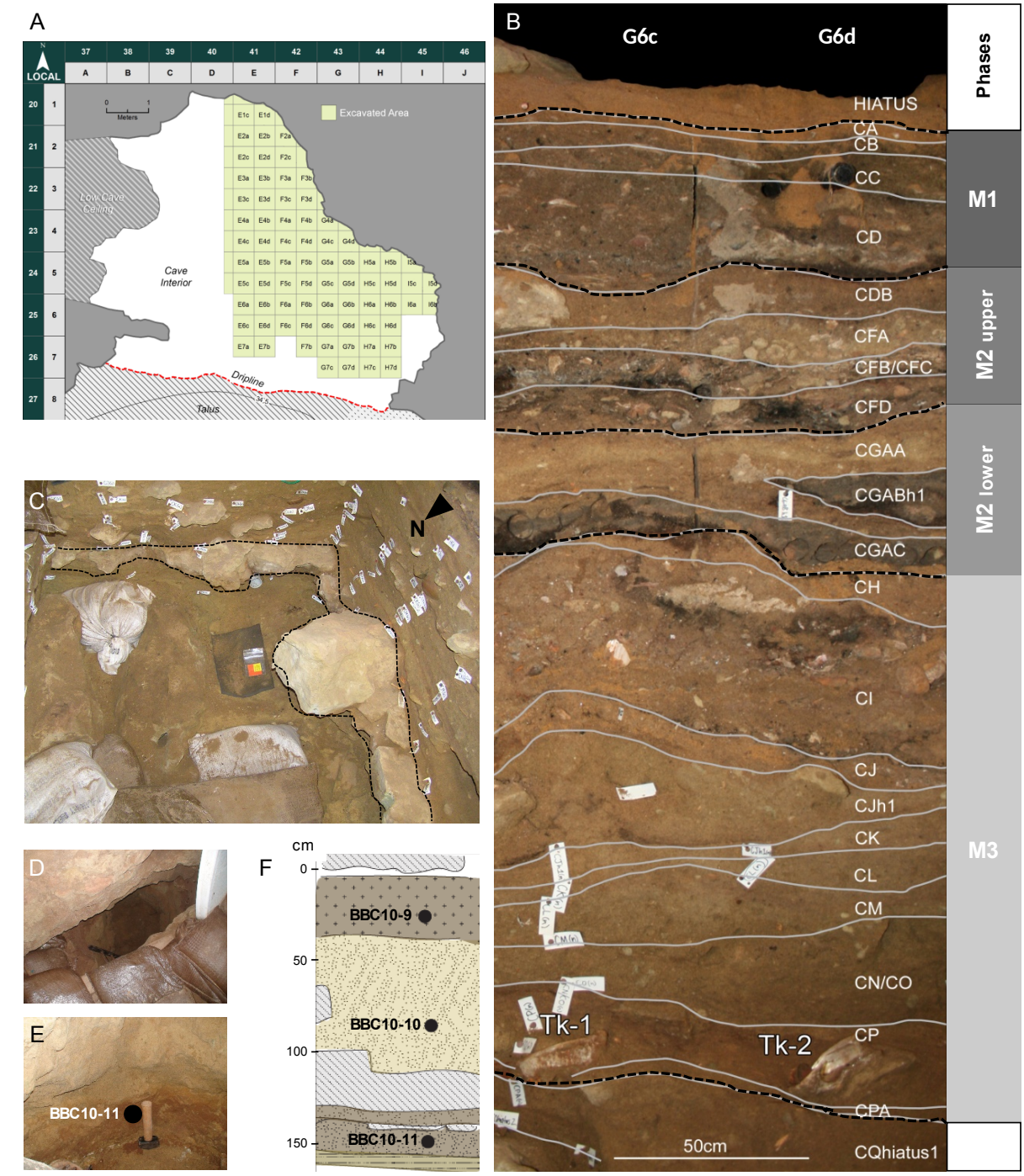
A
LOCAL
Excavated Area
Low Cave Ceiling
Cave Interior
Dripline
Talus
B
G6c
G6d
Phases
HIATUS
CA
CB
CC
CD
CDB
CFA
CFB/CFC
CFD
CGAA
CGABh1
CGAC
CH
CI
CJ
CJh1
CK
CL
CM
CN/CO
CP
CPA
CQhiatus1
M1
M2 upper
M2 lower
M3
Tk-1
Tk-2
50cm
C
N
D
E
BBC10-11
F
cm
0
50
100
150
BBC10-9
BBC10-10
BBC10-11

Figure 2:


7
6
5
8
9
11
10
4
3
1
2
13
15
20
Blombos Cave
TD
LD
WF
0
500 m
Image © 2016 DigitalGlobe
Google earth

Figure 3:

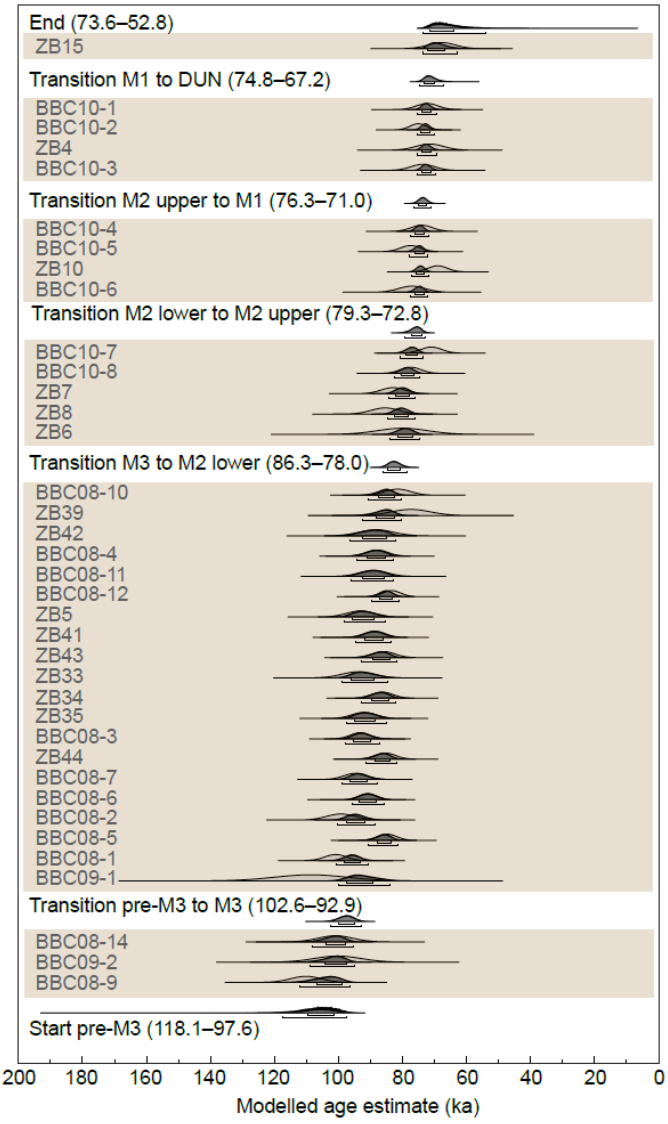
End (73.6–52.8)
ZB15
Transition M1 to DUN (74.8–67.2)
BBC10-1
BBC10-2
ZB4
BBC10-3
Transition M2 upper to M1 (76.3–71.0)
BBC10-4
BBC10-5
ZB10
BBC10-6
Transition M2 lower to M2 upper (79.3–72.8)
BBC10-7
BBC10-8
ZB7
ZB8
ZB6
Transition M3 to M2 lower (86.3–78.0)
BBC08-10
ZB39
ZB42
BBC08-4
BBC08-11
BBC08-12
ZB5
ZB41
ZB43
ZB33
ZB34
ZB35
BBC08-3
ZB44
BBC08-7
BBC08-6
BBC08-2
BBC08-5
BBC08-1
BBC09-1
Transition pre-M3 to M3 (102.6–92.9)
BBC08-14
BBC09-2
BBC08-9
Start pre-M3 (118.1–97.6)
200
180
160
140
120
100
80
60
40
20
0
Modelled age estimate (ka)

Figure 4:

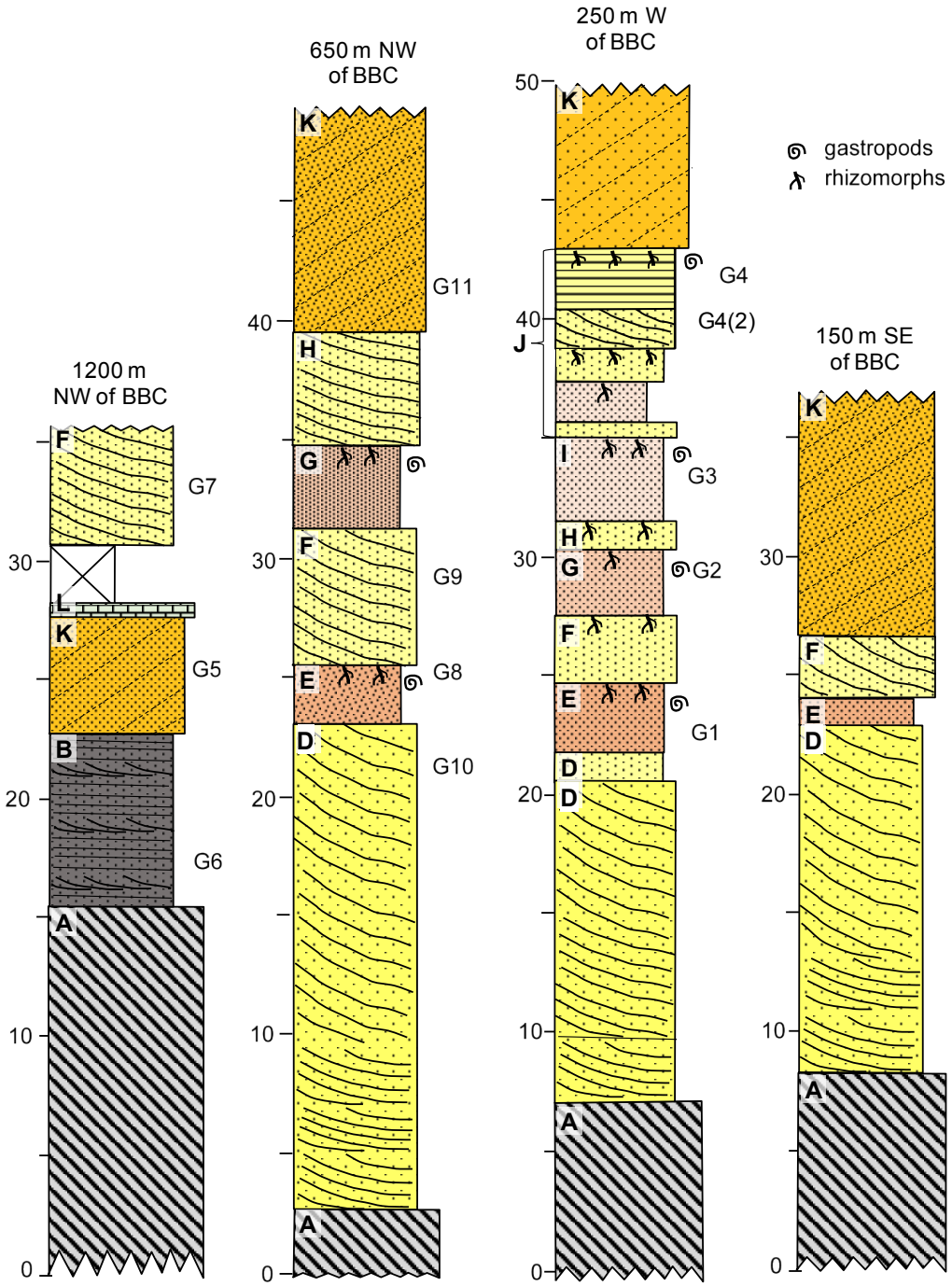
1200 m
NW of BBC
650 m NW
of BBC
250 m W
of BBC
150 m SE
of BBC
gastropods
rhizomorphs
G1
G2
G3
G4
G4(2)
G5
G6
G7
G8
G9
G10
G11
A
B
D
E
F
G
H
I
J
K
L
0
10
20
30
40
50

Figure 5:

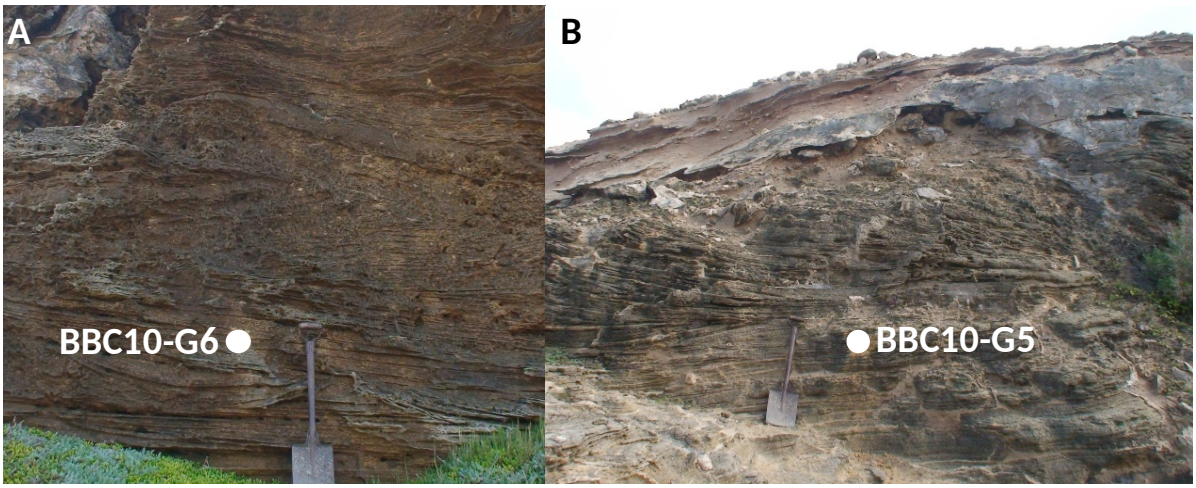


Figure 6:

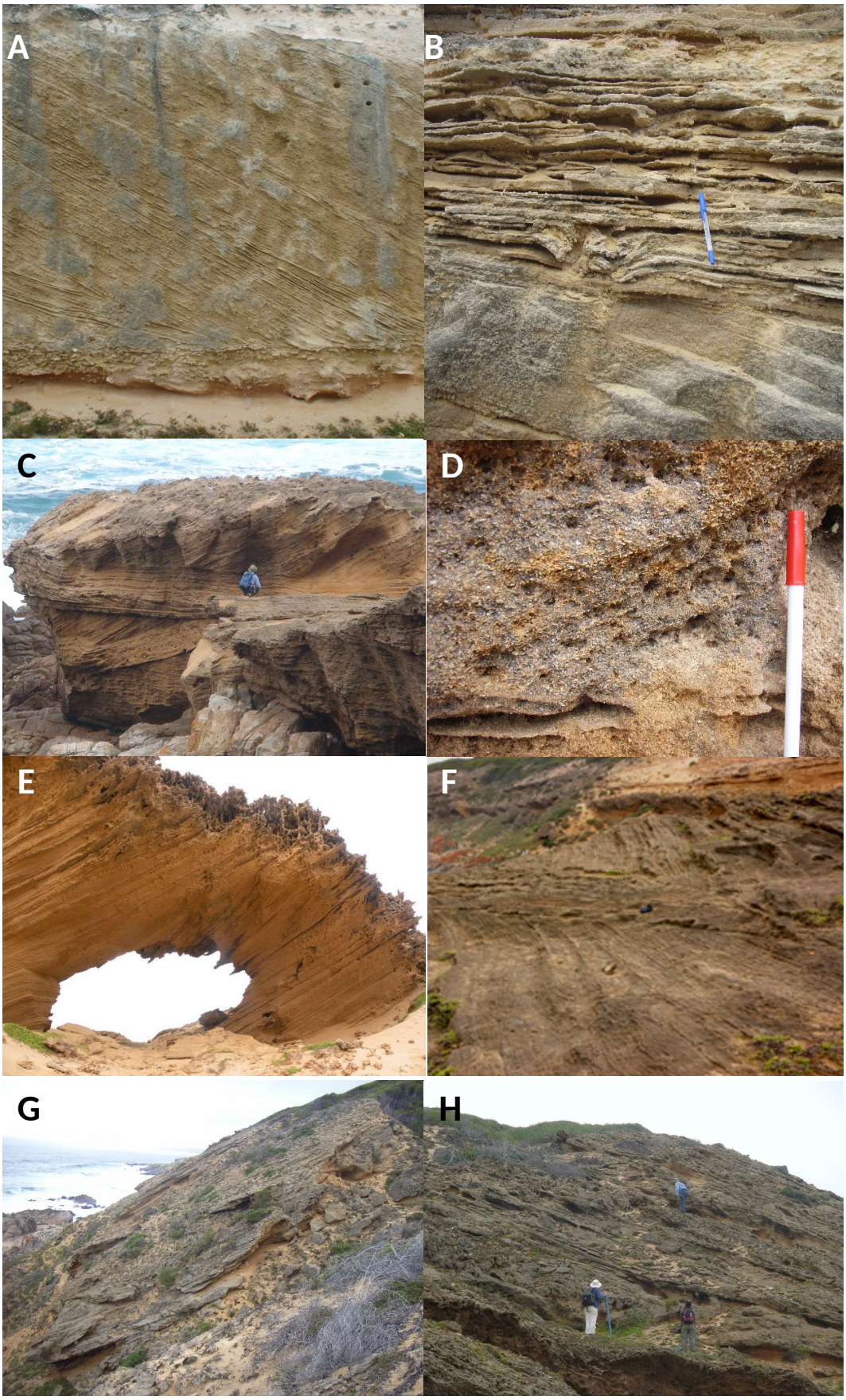


Figure 7:

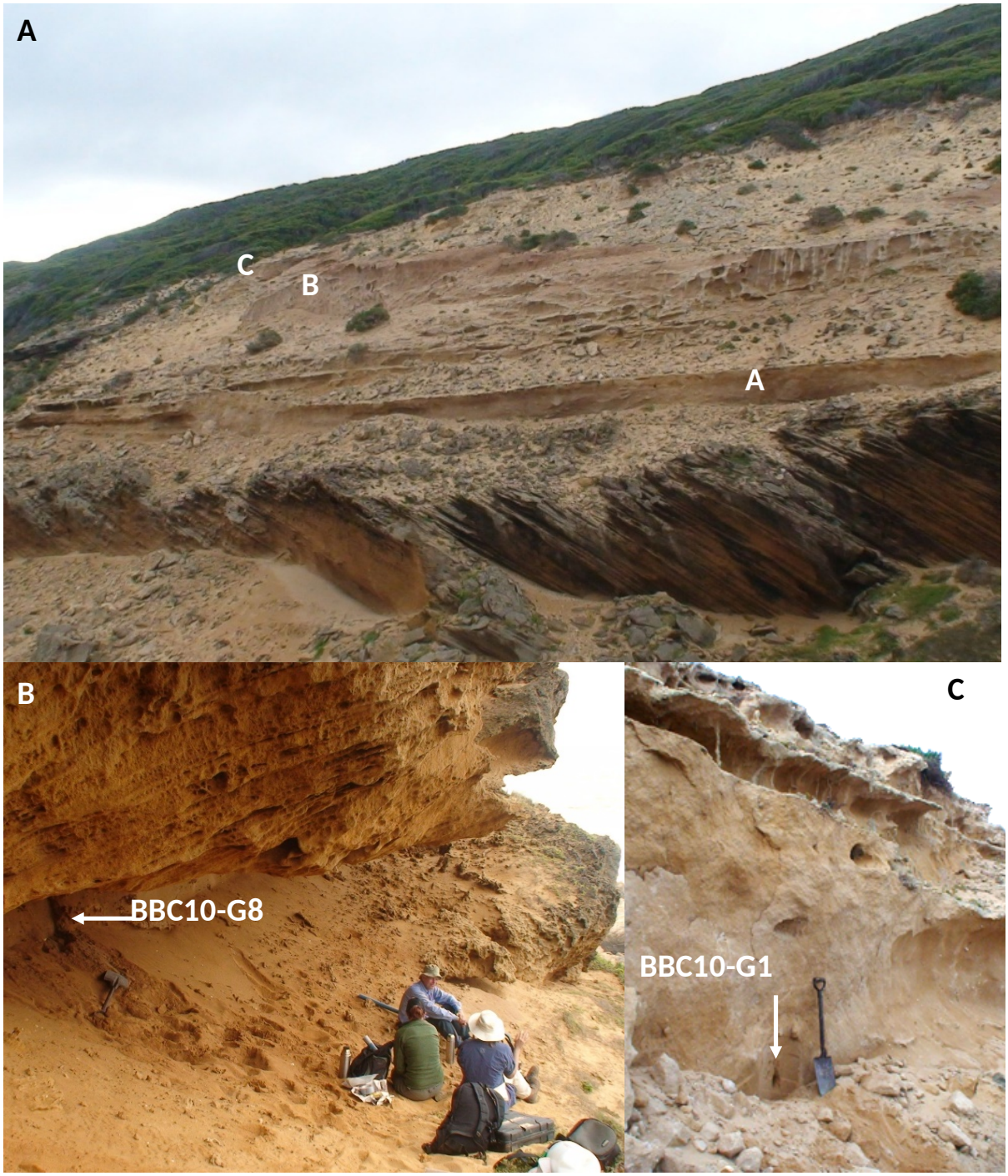


Figure 8:

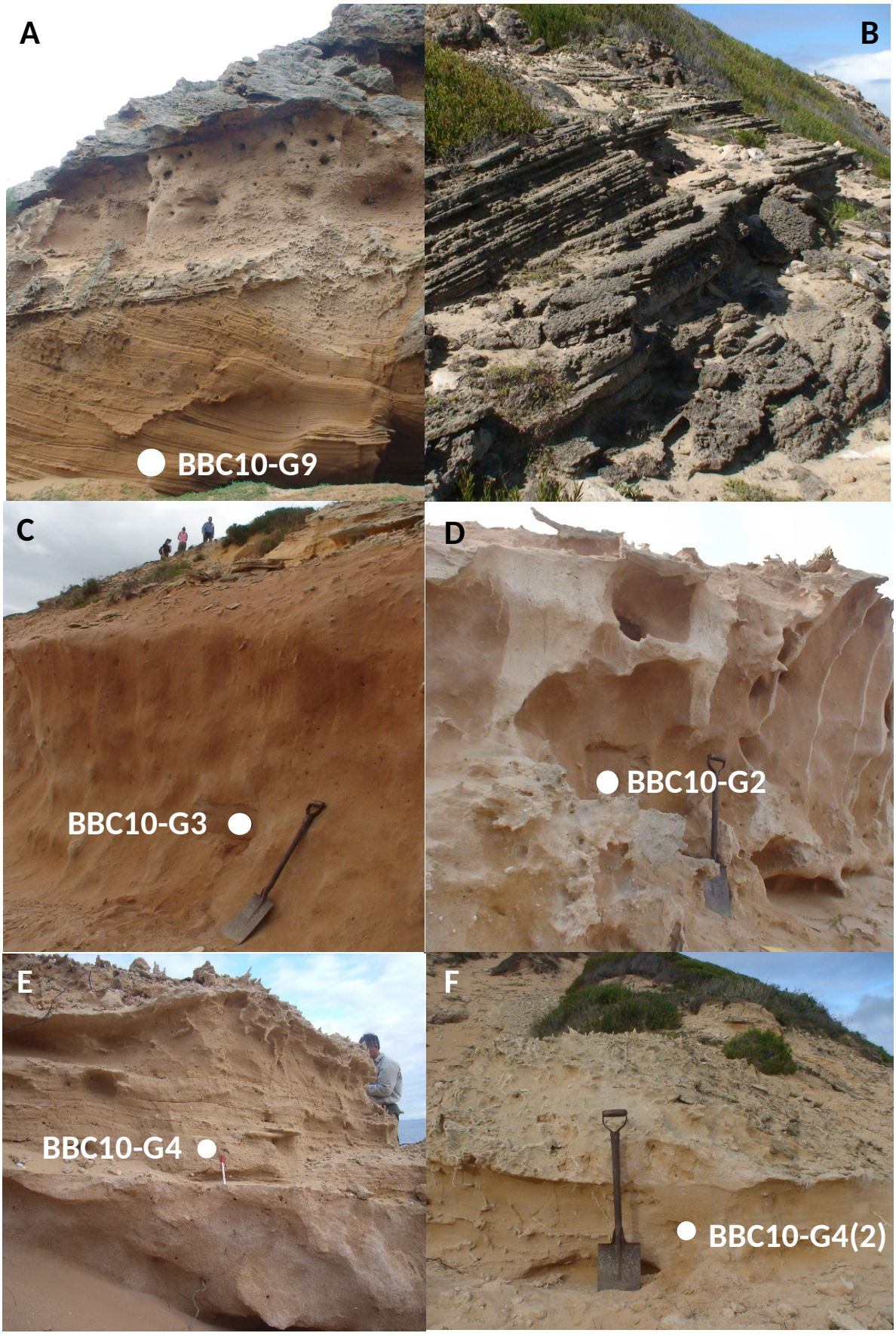


Figure 9:

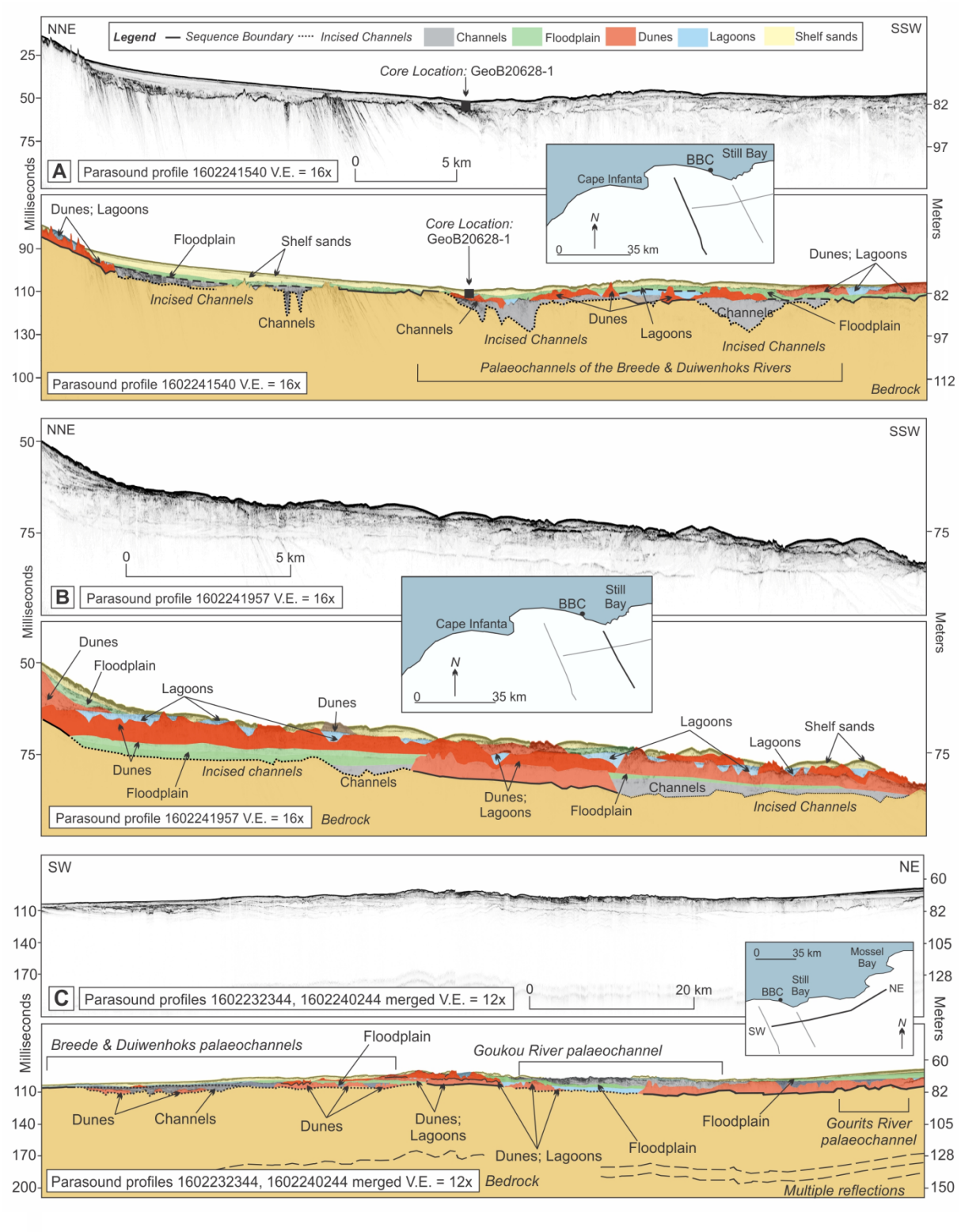
NNE
SSW
Legend — Sequence Boundary ····· Incised Channels
Channels
Floodplain
Dunes
Lagoons
Shelf sands
Core Location: GeoB20628-1
A
Parasound profile 1602241540 V.E. = 16x
0
5 km
Cape Infanta
BBC
Still Bay
N
0
35 km
Milliseconds
Meters
Dunes; Lagoons
Floodplain
Shelf sands
Core Location:
GeoB20628-1
Incised Channels
Channels
Channels
Incised Channels
Dunes
Lagoons
Channels
Incised Channels
Floodplain
Dunes; Lagoons
Palaeochannels of the Breede & Duiwenhoks Rivers
Bedrock
Parasound profile 1602241540 V.E. = 16x
NNE
SSW
0
5 km
B
Parasound profile 1602241957 V.E. = 16x
Cape Infanta
BBC
Still Bay
N
0
35 km
Milliseconds
Meters
Dunes
Floodplain
Lagoons
Dunes
Dunes
Floodplain
Incised channels
Channels
Dunes;
Lagoons
Floodplain
Channels
Incised Channels
Lagoons
Lagoons
Shelf sands
Parasound profile 1602241957 V.E. = 16x
Bedrock
SW
NE
C
Parasound profiles 1602232344, 1602240244 merged V.E. = 12x
0
20 km
0
35 km
Mossel Bay
Still Bay
BBC
NE
SW
N
Milliseconds
Meters
Breede & Duiwenhoks palaeochannels
Floodplain
Goukou River palaeochannel
Dunes
Channels
Dunes
Dunes;
Lagoons
Dunes; Lagoons
Floodplain
Floodplain
Gourits River
palaeochannel
Parasound profiles 1602232344, 1602240244 merged V.E. = 12x
Bedrock
Multiple reflections

Figure 10:

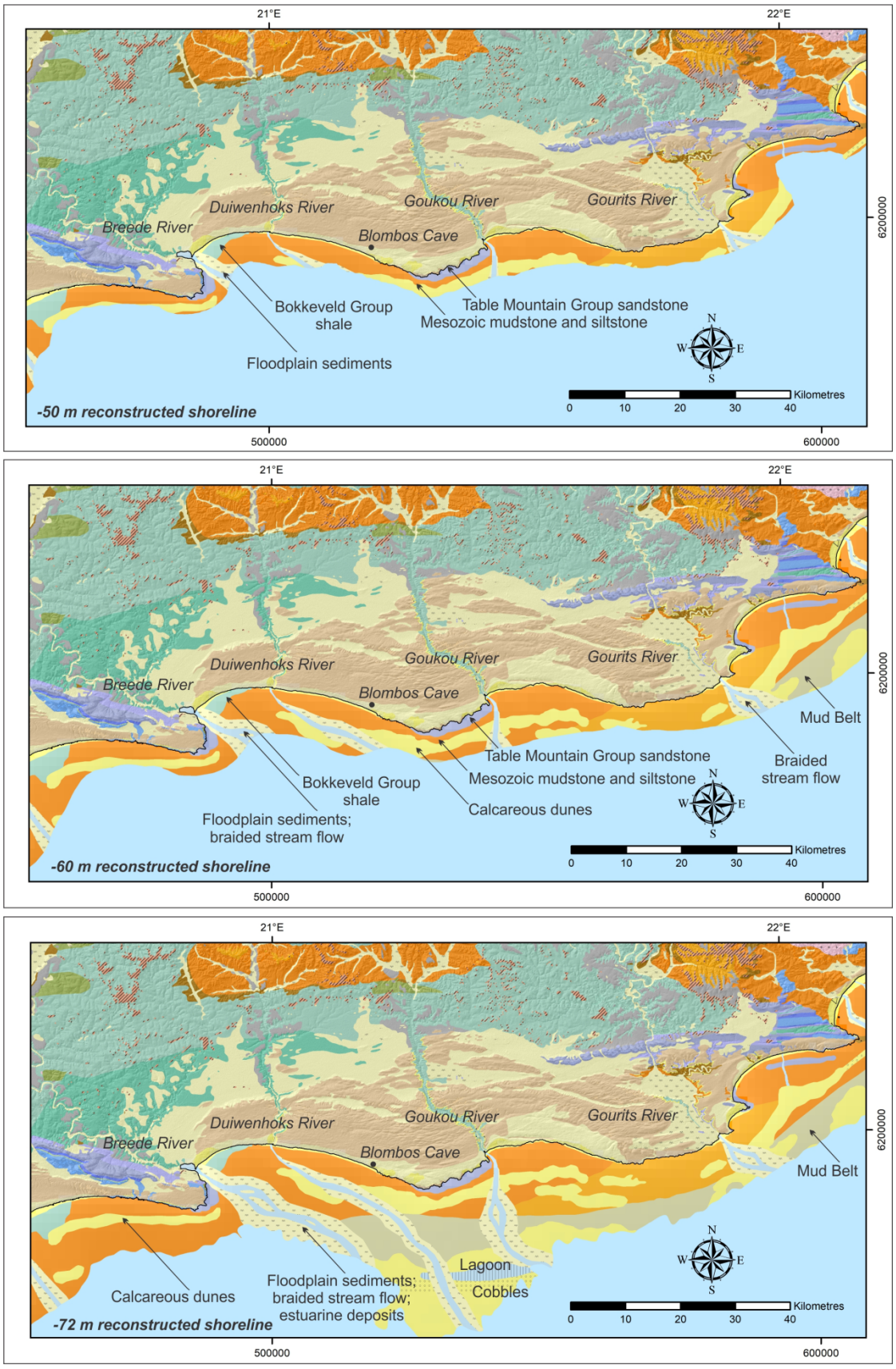
21°E
22°E
Duiwenhoks River
Goukou River
Gourits River
Breede River
Blombos Cave
Bokkeveld Group shale
Table Mountain Group sandstone
Mesozoic mudstone and siltstone
Floodplain sediments
-50 m reconstructed shoreline
N
W
E
S
0 10 20 30 40
Kilometres
500000
600000
6200000
Mud Belt
Braided stream flow
Floodplain sediments; braided stream flow
Calcareous dunes
-60 m reconstructed shoreline
Lagoon
Cobbles
Floodplain sediments; braided stream flow; estuarine deposits
-72 m reconstructed shoreline

Figure 11:

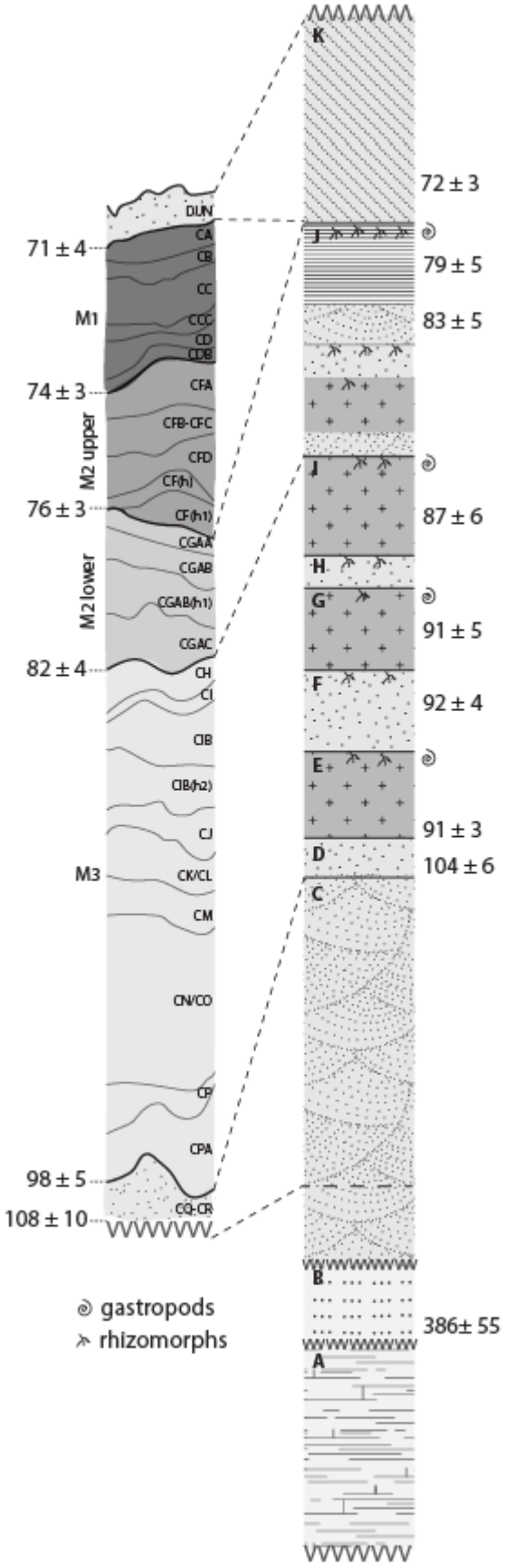
DLN
CA
CB
CC
CCC
CD
CDB
CFA
CFB-CFC
CFD
CF(h)
CF(h1)
CGAA
CGAB
CGAB(h1)
CGAC
CH
CI
CIB
CIB(h2)
CJ
CK/CL
CM
CN/CO
CP
CPA
CQ-CR
M1
M2 upper
M2 lower
M3
71 ± 4
74 ± 3
76 ± 3
82 ± 4
98 ± 5
108 ± 10
K
J
H
G
F
E
D
C
B
A
72 ± 3
79 ± 5
83 ± 5
87 ± 6
91 ± 5
92 ± 4
91 ± 3
104 ± 6
386± 55
gastropods
rhizomorphs

Figure 12:

Table 1:

| Sample | Layer | Square | Water content (%) | Environmental dose rate (Gy/ka) | | | | $D_e$ value (Gy) | Over-dispersion (%) | Number of grains | Age ± σ2 |
|---|---|---|---|---|---|---|---|---|---|---|---|
| | | | | Beta [b] | Gamma | Cosmic | Total | | | | |
| ZB15 | DUN | | 5 | 0.34 ± 0.02 | 0.31 ± 0.02 | 0.05 | 0.73 ± 0.03 | 49.2 ± 2.1 | 15 ± 3 | 34/1000 | 67.8 ± 4.2 |
| **M1 PHASE** | | | | | | | | | | | |
| BBC10-1 | CA | H6d | 6 | 0.57 ± 0.03 | 0.42 ± 0.02 | 0.04 | 1.06 ± 0.04 | 76.3 ± 2.7 | 20 ± 4 | 93/1000 | 72.3 ± 3.8 (3.3) |
| BBC10-2 | CC | H6d | 6 | 0.58 ± 0.03 | 0.47 ± 0.02 | 0.04 | 1.12 ± 0.04 | 83.7 ± 1.7 | 25 ± 2 | 311/3000 | 75.1 ± 3.2 (2.5) |
| ZB4 | CC | G6d | 11 | 0.57 ± 0.03 | 0.44 ± 0.02 | 0.04 | 1.08 ± 0.04 | 77.6 ± 2.7 | 18 ± 3 | 122/1000 | 71.5 ± 4.3 |
| BBC10-3 | CD | H6d | 7 | 0.61 ± 0.03 | 0.43 ± 0.02 | 0.04 | 1.11 ± 0.04 | 81.8 ± 3.4 | 26 ± 4 | 81/1000 | 73.7 ± 4.2 (3.7) |
| **M2 upper PHASE** | | | | | | | | | | | |
| BBC10-4 | CFA | H6d | 6 | 0.59 ± 0.03 | 0.37 ± 0.02 | 0.04 | 1.03 ± 0.04 | 76.4 ± 2.7 | 14 ± 2 | 149/1000 | 74.0 ± 3.9 (3.3) |
| BBC10-5 | CFB/CFC | H6d | 8 | 0.54 ± 0.03 | 0.41 ± 0.03 | 0.04 | 1.02 ± 0.04 | 78.8 ± 1.9 | 26 ± 2 | 206/2000 | 77.5 ± 3.8 (3.1) |
| BBC10-6 | CFB/CFC | H6d | 13 | 0.56 ± 0.03 | 0.47 ± 0.03 | 0.04 | 1.09 ± 0.04 | 75.5 ± 3.0 | 25 ± 2 | 124/1000 | 69.0 ± 4.0 (3.0) |
| ZB10 | CFD | H6c | 6 | 0.58 ± 0.03 | 0.40 ± 0.03 | 0.04 | 1.04 ± 0.04 | 80.2 ± 2.9 | 25 ± 6 | 113/1000 | 77.1 ± 4.1 |
| **M2 lower PHASE** | | | | | | | | | | | |
| BBC10-7 | CGAA | H6d | 20 | 0.67 ± 0.04 | 0.48 ± 0.03 | 0.04 | 1.21 ± 0.05 | 85.8 ± 3.2 | 16 ± 1 | 499/2000 | 71.0 ± 4.0 (3.2) |
| BBC10-8 | CGAA | H6d | 10 | 0.59 ± 0.03 | 0.45 ± 0.03 | 0.04 | 1.10 ± 0.04 | 85.2 ± 2.5 | 17 ± 3 | 339/2000 | 77.4 ± 4.2 (3.2) |
| ZB7 | CGAA | F6b | 11 | 0.54 ± 0.03 | 0.43 ± 0.03 | 0.04 | 1.05 ± 0.04 | 87.0 ± 2.2 | 21 ± 1 | 92/1000 | 82.9 ± 3.8 |
| ZB8 | CGAB/CGAC | G6b | 17 | 0.58 ± 0.05 | 0.43 ± 0.02 | 0.04 | 1.09 ± 0.05 | 93.2 ± 2.0 | 29 ± 2 | 307/2400 | 85.5 ± 4.3 |
| ZB6 | CGAC | G6b | 8 | 0.79 ± 0.04 | 0.33 ± 0.04 | 0.04 | 1.20 ± 0.05 | 96.0 ± 8.5 | 12 ± 2 | 51/1000 | 80.0 ± 7.8 |
| **M3 PHASE** | | | | | | | | | | | |
| BBC08-10 | CH | F6c | 8 | 0.65 ± 0.03 | 0.34 ± 0.02 | 0.03 | 1.05 ± 0.03 | 85.2 ± 3.7 | 17 ± 3 | 123/1000 | 81.5 ± 4.7 (4.0) |
| ZB39 | CH | F6d | 10 | 0.55 ± 0.06 | 0.34 ± 0.02 | 0.03 | 0.96 ± 0.06 | 73.9 ± 3.7 | | 58/500 | 77.4 ± 6.5 (6.1) |
| ZB42 | CH/CI | I4c | 11 | 0.67 ± 0.04 | 0.50 ± 0.04 | 0.03 | 1.23 ± 0.06 | 108.7 ± 3.5 | 21 | 85/1700 | 88.2 ± 5.3 |
| BBC08-4 | CIB | G6c | 2.2 | 0.70 ± 0.03 | 0.34 ± 0.01 | 0.03 | 1.10 ± 0.04 | 97.1 ± 2.3 | 21 ± 2 | 213/1000 | 88.0 ± 3.9 (3.4) |
| BBC08-11 | CIB | F6c | 16.4 | 0.58 ± 0.03 | 0.38 ± 0.02 | 0.03 | 1.03 ± 0.03 | 91.4 ± 3.8 | 24 ± 3 | 123/1000 | 89.1 ± 5.1 (4.3) |
| BBC08-12 | CIBh1 | D5d | 3.2 | 0.73 ± 0.03 | 0.31 ± 0.01 | 0.03 | 1.11 ± 0.04 | 92.3 ± 2.3 | 27 ± 2 | 245/1000 | 83.4 ± 3.8 (2.8) |
| ZB5 | CJ | H5d | 5 | 0.99 ± 0.05 | 0.54 ± 0.02 | 0.03 | 1.59 ± 0.06 | 148.9 ± 4.7 | 15 ± 4 | 89/1000 | 93.2 ± 4.3 |

| | | | | | | | | | | | |
|---|---|---|---|---|---|---|---|---|---|---|---|
| ZB41 | CJ | F6d | 3 | 0.63 ± 0.03 | 0.46 ± 0.03 | 0.03 | 1.16 ± 0.04 | 102.6 ± 2.6 | 18 ± 3 | 133/1000 | 88.7 ± 4.2 (3.2) |
| ZB43 | CJ | H5d | 3 | 0.92 ± 0.04 | 0.50 ± 0.02 | 0.03 | 1.49 ± 0.04 | 127.8 ± 4.0 | 21 ± 3 | 120/1000 | 85.9 ± 4.1 (3.5) |
| ZB33 | CJ | | 5 | 0.56 ± 0.03 | 0.46 ± 0.02 | 0.03 | 1.09 ± 0.04 | 102.2 ± 4.6 | 20 ± 5 | 63/400 | 94.0 ± 5.6 (5.0) |
| ZB34 | CJ | | 5 | 0.68 ± 0.03 | 0.54 ± 0.03 | 0.03 | 1.28 ± 0.04 | 110.2 ± 3.4 | 15 ± 3 | 81/700 | 86.3 ± 4.2 (3.3) |
| ZB35 | CJ | | 5 | 0.56 ± 0.03 | 0.49 ± 0.03 | 0.03 | 1.12 ± 0.04 | 102.4 ± 3.0 | 11 ± 4 | 93/500 | 92.1 ± 4.6 (3.8) |
| BBC08-3 | CJh1 | G6c | 2 | 0.62 ± 0.03 | 0.33 ± 0.01 | 0.03 | 1.01 ± 0.03 | 94.4 ± 2.0 | 18 ± 2 | 244/1000 | 93.3 ± 4.1 (3.0) |
| ZB44 | CJh1 | F6d | 3 | 0.83 ± 0.03 | 0.42 ± 0.02 | 0.03 | 1.31 ± 0.04 | 111.6 ± 3.4 | 30 ± 3 | 203/900 | 85.3 ± 4.0 (3.1) |
| BBC08-7 | CO | G6b | 7 | 0.77 ± 0.04 | 0.44 ± 0.02 | 0.03 | 1.27 ± 0.05 | 120.6 ± 3.3 | 25 ± 3 | 194/1000 | 94.9 ± 4.8 (3.4) |
| BBC08-6 | CP upper | G6b | 3 | 1.07 ± 0.04 | 0.43 ± 0.02 | 0.03 | 1.56 ± 0.05 | 141.9 ± 3.6 | 21 ± 3 | 183/1000 | 90.9 ± 4.3 (2.8) |
| BBC08-2 | CP/CPA | G6b | 2 | 0.61 ± 0.03 | 0.42 ± 0.02 | 0.03 | 1.10 ± 0.04 | 108.7 ± 3.4 | 30 ± 3 | 183/1000 | 99.3 ± 5.0 (4.4) |
| BBC08-5 | CP/CPA | G6c | 4 | 0.73 ± 0.03 | 0.37 ± 0.02 | 0.03 | 1.16 ± 0.04 | 98.3 ± 2.5 | 24 ± 3 | 222/1000 | 84.7 ± 3.9 (2.9) |
| BBC08-1 | CP/CPA | G6d | 1 | 0.58 ± 0.03 | 0.40 ± 0.02 | 0.03 | 1.03 ± 0.03 | 104.4 ± 2.6 | 19 ± 3 | 209/1000 | 100.9 ± 4.6 (3.4) |
| BBC09-1 | CPA | F6a | 3 | 0.63 ± 0.03 | 0.45 ± 0.03 | 0.03 | 1.14 ± 0.04 | 124.4 ± 12.5 | 37 ± 5 | 30/500 | 108.7 ± 11.8 (11.4) |
| **Pre-M3 PHASE** | | | | | | | | | | | |
| BBC08-14 | CQ–CR | H6b | 3 | 0.70 ± 0.03 | 0.43 ± 0.02 | 0.03 | 1.20 ± 0.04 | 120.7 ± 5.5 | 17 ± 10 | 97/1000 | 101.0 ± 6.0 (5.3) |
| BBC09-2 | CQ–CR | F5d | 1 | 0.67 ± 0.03 | 0.44 ± 0.02 | 0.03 | 1.17 ± 0.04 | 117.1 ± 7.8 | 41 ± 23 | 58/1000 | 100.3 ± 7.6 (7.2) |
| BBC08-9 | CR | I6b | 2 | 0.73 ± 0.03 | 0.41 ± 0.02 | 0.03 | 1.21 ± 0.04 | 133.1 ± 3.0 | 13 ± 3 | 181/1000 | 110.2 ± 4.8 (3.4) |
| **INNER CHAMBER** | | | | | | | | | | | |
| BBC10-9 | | | 15 | 0.55 ± 0.03 | 0.39 ± 0.03 | 0.02 | 0.99 ± 0.04 | 85.7 ± 3.7 | 8 ± 4 | 201/1000 | 86.6 ± 5.5 (4.6) |
| BBC10-10 | | | 20 | 0.74 ± 0.05 | 0.47 ± 0.03 | 0.02 | 1.26 ± 0.05 | 124.2 ± 3.5 | 9 ± 1 | 140/1000 | 98.9 ± 5.1 (3.7) |
| BBC10-11 | | | 30 | 1.15 ± 0.07 | 0.76 ± 0.05 | 0.02 | 1.96 ± 0.09 | 250.0 ± 30.8 | 23 ± 9 | 166/1000 | 127.5 ± 16.9 (16.1) |

Table 2:

| Sample | UNMODELLED AGE RANGES (years) | | | | MODELLED AGE RANGES (years) | | | | Outlier Probabilities (%) | | Convergence Values (%) |
|---|---|---|---|---|---|---|---|---|---|---|---|
| | 68.2% probability | | 95.4% probability | | 68.2% probability | | 95.4% probability | | | | |
| | from | to | from | to | from | to | from | to | prior | posterior | |
| ***End of DUN*** | | | | | ***71,850*** | ***63,010*** | ***73,620*** | ***52,760*** | | | ***84*** |
| ZB15 | 72,000 | 63,610 | 76,180 | 59,420 | 72,130 | 66,830 | 73,720 | 62,920 | 5 | 5 | 98.6 |
| ***Transition between M1 and DUN*** | | | | | ***73,460*** | ***69,860*** | ***74,820*** | ***67,240*** | | | ***98.6*** |
| BBC10-1 | 75,600 | 69,000 | 78,890 | 65,720 | 74,100 | 71,200 | 75,400 | 69,470 | 5 | 5 | 99.6 |
| BBC10-2 | 77,600 | 72,600 | 80,090 | 70,110 | 74,200 | 71,510 | 75,460 | 70,060 | 5 | 5 | 99.6 |
| ZB4 | 75,800 | 67,210 | 80,080 | 62,920 | 74,100 | 71,150 | 75,430 | 69,290 | 5 | 5 | 99.5 |
| BBC10-3 | 77,400 | 70,010 | 81,080 | 66,320 | 74,150 | 71,250 | 75,450 | 69,560 | 5 | 5 | 99.6 |
| ***Transition between M2 upper and M1*** | | | | | 75,040 | 72,330 | 76,300 | 71,000 | | | 99.4 |
| BBC10-4 | 77,300 | 70,700 | 80,590 | 67,420 | 76,000 | 73,230 | 77,480 | 71,990 | 5 | 5 | 99.6 |
| BBC10-5 | 80,600 | 74,400 | 83,690 | 71,320 | 76,200 | 73,390 | 77,820 | 72,130 | 5 | 5 | 99.5 |
| BBC10-6 | 72,000 | 66,000 | 74,990 | 63,020 | 75,710 | 73,070 | 77,060 | 71,770 | 5 | 6 | 99.5 |
| ZB10 | 81,200 | 73,010 | 85,280 | 68,920 | 76,140 | 73,290 | 77,770 | 72,020 | 5 | 5 | 99.6 |
| ***Transition between M2 lower and M2 upper*** | | | | | ***77,260*** | ***74,040*** | ***79,260*** | ***72,750*** | | | ***99.1*** |
| BBC10-7 | 74,200 | 67,800 | 77,390 | 64,620 | 78,890 | 75,180 | 80,880 | 73,780 | 5 | 7 | 98.8 |
| BBC10-8 | 80,600 | 74,200 | 83,790 | 71,020 | 80,560 | 76,470 | 82,540 | 74,810 | 5 | 5 | 99.3 |
| ZB7 | 86,700 | 79,110 | 90,480 | 75,320 | 82,270 | 77,870 | 84,190 | 75,930 | 5 | 5 | 99.2 |
| ZB8 | 89,800 | 81,210 | 94,080 | 76,920 | 82,560 | 78,190 | 84,550 | 76,120 | 5 | 5 | 99.1 |
| ZB6 | 87,790 | 72,210 | 95,570 | 64,440 | 81,580 | 76,750 | 83,830 | 74,770 | 5 | 5 | 99.3 |
| ***Transition between M3 and M2 lower*** | | | | | ***84,580*** | ***80,750*** | ***86,280*** | ***78,700*** | | | ***99.2*** |
| BBC08-10 | 85,500 | 77,510 | 89,480 | 73,520 | 87,720 | 82,590 | 90,840 | 80,550 | 5 | 5 | 98.2 |
| ZB39 | 83,490 | 71,310 | 89,570 | 65,230 | 88,400 | 82,380 | 92,480 | 80,210 | 5 | 5 | 98 |
| ZB42 | 93,500 | 82,910 | 98,780 | 77,630 | 92,660 | 84,790 | 96,460 | 82,200 | 5 | 5 | 98.6 |
| BBC08-4 | 91,400 | 84,600 | 94,790 | 81,220 | 91,200 | 85,110 | 94,360 | 82,890 | 5 | 5 | 98.6 |
| BBC08-11 | 93,400 | 84,810 | 97,680 | 80,520 | 92,830 | 85,580 | 96,080 | 82,960 | 5 | 5 | 98.5 |
| BBC08-12 | 86,200 | 80,600 | 88,990 | 77,810 | 87,300 | 82,970 | 89,700 | 81,050 | 5 | 5 | 98.4 |

| | | | | | | | | | | | |
|---|---|---|---|---|---|---|---|---|---|---|---|
| ZB5 | 97,500 | 88,910 | 101,780 | 84,620 | 95,720 | 88,770 | 98,270 | 85,280 | 5 | 5 | 98.5 |
| ZB41 | 91,900 | 85,500 | 95,090 | 82,320 | 91,750 | 85,770 | 94,620 | 83,440 | 5 | 5 | 98.5 |
| ZB43 | 89,400 | 82,400 | 92,890 | 78,920 | 89,590 | 83,930 | 92,840 | 81,780 | 5 | 5 | 98.5 |
| ZB33 | 99,000 | 89,010 | 103,980 | 84,020 | 96,130 | 88,770 | 98,750 | 84,760 | 5 | 5 | 98.4 |
| ZB34 | 89,600 | 83,000 | 92,890 | 79,720 | 89,730 | 84,170 | 92,740 | 82,040 | 5 | 5 | 98.4 |
| ZB35 | 95,900 | 88,310 | 99,680 | 84,520 | 94,970 | 88,370 | 97,550 | 85,060 | 5 | 5 | 98.5 |
| BBC08-3 | 96,300 | 90,300 | 99,290 | 87,320 | 95,460 | 90,080 | 97,780 | 87,290 | 5 | 5 | 98.4 |
| ZB44 | 88,400 | 82,200 | 91,490 | 79,120 | 88,760 | 83,680 | 91,590 | 81,710 | 5 | 5 | 98.5 |
| BBC08-7 | 98,300 | 91,500 | 101,690 | 88,120 | 96,420 | 90,820 | 98,770 | 87,790 | 5 | 5 | 98.3 |
| BBC08-6 | 93,700 | 88,100 | 96,490 | 85,310 | 93,540 | 88,100 | 95,870 | 85,590 | 5 | 5 | 98.5 |
| BBC08-2 | 103,700 | 94,910 | 108,080 | 90,520 | 97,740 | 91,870 | 100,300 | 88,540 | 5 | 5 | 97.9 |
| BBC08-5 | 87,600 | 81,800 | 90,490 | 78,910 | 88,130 | 83,470 | 90,800 | 81,540 | 5 | 5 | 98.4 |
| BBC08-1 | 104,300 | 97,500 | 107,690 | 94,120 | 98,250 | 93,190 | 100,760 | 90,660 | 5 | 6 | 97.6 |
| BBC09-1 | 120,090 | 97,320 | 131,450 | 85,950 | 97,580 | 88,920 | 100,030 | 83,940 | 5 | 5 | 98.2 |
| ***Transition between pre-M3 and M3*** | | | | | ***99,990*** | ***95,070*** | ***102,610*** | ***92,870*** | | | ***98.2*** |
| BBC08-14 | 106,300 | | 111,580 | 90,430 | 104,170 | 97,860 | 108,110 | 95,500 | 5 | 5 | 98.8 |
| BBC09-2 | 107,490 | | 114,670 | 85,930 | 104,280 | 97,560 | 108,960 | 95,130 | 5 | 5 | 98.7 |
| BBC08-9 | 115,000 | | 119,780 | 100,620 | 107,030 | 99,000 | 112,200 | 96,490 | 5 | 5 | 97.4 |
| ***Start of pre-M3*** | | | | | ***111,120*** | ***99,850*** | ***118,140*** | ***97,550*** | | | ***69.9*** |

Table 3:

| **Unit** | **Basal sand** | **Lower dunes** | | | | | **Soils** | | | | **Upper dunes** | | **Calcrete** |
|---|---|---|---|---|---|---|---|---|---|---|---|---|---|
| Sample (BBC10-) | G6* | G10* | G7 | G9 | G4(2) | G4 | G1 | G8 | G2 | G3 | G5 | G11 | |
| Sand (%) | 95.8 | 95.7 | 92.2 | 93.1 | 96.3 | 92.8 | 90.5 | 86.6 | 89.5 | 84.7 | 95.3 | 90.9 | – |
| Mean size (µm) | 204 | 398 | 663 | 438 | 274 | 390 | 380 | 355 | 433 | 398 | 385 | 580 | – |
| Quartz | 90.9 | 94.5 | 68.6 | 48.4 | 72.5 | 72.1 | 68.4 | 74.3 | 77.2 | 81.7 | 50.9 | 48.7 | 35.3 |
| Plagioclase | 1.6 | 2.1 | 1.5 | 1.6 | 2.2 | 3.2 | 3.4 | 2.5 | 3.2 | 4.7 | 1.8 | 1.6 | 4.0 |
| K-feldspar | 5.6 | – | 3.9 | – | – | – | – | – | – | – | – | 0.4 | – |
| Calcite | – | 0.1 | 21.4 | 45.2 | 19.3 | 16.5 | 14.2 | 13.3 | 11.7 | 7.5 | 42.8 | 47.7 | 51.4 |
| High Mg calcite | – | 0.2 | 0.9 | 2.7 | 2.5 | 3.8 | 7.2 | 4.4 | 3.5 | 2.1 | 2.2 | 0.9 | 4.0 |
| Kaolinite | 0.6 | 1.0 | 1.1 | – | 0.4 | 0.7 | 1.0 | 0.7 | 0.5 | – | – | – | – |
| Illite | 1.3 | 2.0 | 2.5 | 2.1 | 3.2 | 3.7 | 5.7 | 4.6 | 3.8 | 4.1 | 2.3 | 0.6 | 5.2 |

Samples with an asterisk (*) were acid leached.

Table 4:

| Sample name | Moisture content (%) | Dose rates (Gy/ka) | | | Total dose rate (Gy/ka) | $D_e$ (Gy) | Number of aliquots | OD (%) | OSL age (ka) |
|---|---|---|---|---|---|---|---|---|---|
| | | Beta | Gamma | Cosmic | | | | | |
| **Unit K: Top dune** | | | | | | | | | |
| BBC10-G5 | 20 (21.7) | 0.22 ± 0.02 | 0.19 ± 0.02 | 0.046 ± 0.007 | 0.48 ± 0.03 | 35.2 ± 1.3 | 24/24 | 16 ± 3 | 72.8 ± 5.2 (4.6) |
| BBC10-G11 | 10 (8.4) | 0.17 ± 0.02 | 0.22 ± 0.02 | 0.064 ± 0.010 | 0.48 ± 0.03 | 34.8 ± 0.6 | 23/24 | 8 ± 2 | 71.9 ± 4.8 (4.2) |
| **Unit J: Above Palaeosol C** | | | | | | | | | |
| BBC10-G4 | 5 (1.9) | 0.17 ± 0.02 | 0.18 ± 0.01 | 0.097 ± 0.019 | 0.47 ± 0.03 | 37.4 ± 0.9 | 24/24 | 11 ± 2 | 79.3 ± 5.9 (4.7) |
| BBC10-G4(2) | 5 (1.4) | 0.17 ± 0.02 | 0.18 ± 0.01 | 0.083 ± 0.017 | 0.46 ± 0.03 | 38.6 ± 0.6 | 24/24 | 10 ± 2 | 83.4 ± 6.0 (4.8) |
| **Unit I: Palaeosol C** | | | | | | | | | |
| BBC10-G3 | 10 (10.5) | 0.16 ± 0.02 | 0.16 ± 0.02 | 0.049 ± 0.010 | 0.40 ± 0.03 | 35.0 ± 0.9 | 24/24 | 11 ± 2 | 87.2 ± 6.5 (5.8) |
| **Unit G: Palaeosol B** | | | | | | | | | |
| BBC10-G2 | 10 (2.4) | 0.20 ± 0.02 | 0.18 ± 0.01 | 0.063 ± 0.009 | 0.46 ± 0.03 | 41.9 ± 0.8 | 24/24 | 9 ± 2 | 90.7 ± 5.8 (5.2) |
| **Unit F: Dune unit between Palaeosols A and B** | | | | | | | | | |
| BBC10-G7 | 10 (7.0) | 0.18 ± 0.02 | 0.17 ± 0.01 | 0.118 ± 0.024 | 0.49 ± 0.03 | 44.4 ± 1.7 | 24/24 | 18 ± 3 | 91.4 ± 7.5 (5.8) |
| BBC10-G9 | 10 (2.4) | 0.22 ± 0.02 | 0.23 ± 0.02 | 0.037 ± 0.007 | 0.49 ± 0.03 | 45.3 ± 1.2 | 24/24 | 12 ± 2 | 93.2 ± 6.3 (5.7) |
| **Unit E: Palaeosol A** | | | | | | | | | |
| BBC10-G1 | 10 (4) | 0.30 ± 0.02 | 0.35 ± 0.03 | 0.037 ± 0.006 | 0.68 ± 0.04 | 63.0 ± 2.1 | 24/24 | 16 ± 3 | 92.5 ± 6.1 (5.5) |
| BBC10-G8 | 10 (8.9) | 0.32 ± 0.02 | 0.31 ± 0.02 | 0.035 ± 0.005 | 0.70 ± 0.03 | 63.1 ± 1.6 | 24/24 | 11 ± 2 | 90.0 ± 5.1 (4.3) |
| **Unit D: Dune unit below Palaeosol A** | | | | | | | | | |
| BBC10-G10 | 20 (19.3) | 0.23 ± 0.02 | 0.24 ± 0.02 | 0.012 ± 0.002 | 0.52 ± 0.03 | 53.8 ± 1.7 | 23/24 | 14 ± 3 | 104.2 ± 7.0 (6.1) |
| **Unit B: Lower thinly bedded sands** | | | | | | | | | |
| BBC10-G6 | 30 (35) | 0.23 ± 0.02 | 0.24 ± 0.02 | 0.019 ± 0.004 | 0.52 ± 0.03 | 200.6 ± 26.6 | 81/1000 | 15 ± 4 | 386.1 ± 56.5 (54.5) |

The total dose rate includes an allowance of 0.029 ± 0.010 Gy/ka for the internal dose rate.